The Astrophysical Journal, 652:774–792, 2006 November 20

ULTRAVIOLET PROPERTIES OF HALO CORONAL MASS EJECTIONS: DOPPLER SHIFTS, ANGLES, SHOCKS, AND BULK MORPHOLOGY

A. Ciaravella,[1,2] J. C. Raymond,[2] and S. W. Kahler[3]
Received 2005 February 25; accepted 2006 June 19

ABSTRACT

We present UV spectral information for 22 halo or partial halo CMEs observed by UVCS. The CME fronts show broad line profiles, while the line intensities are comparable to the background corona. The Doppler shifts of the front material are generally small, showing that the motion of gas in the fronts is mostly transverse to the line of sight. This indicates that, at least in halo CMEs, the fronts generally correspond to coronal plasma swept up by a shock or compression wave, rather than plasma carried outward by magnetic loops. This favors an ice cream cone (or a spherical shell) model, as opposed to an expanding arcade of loops. We use the line widths to discriminate between shock heating and bulk expansion. Of 14 cases where we detected the CME front, the line broadening in 7 cases can be attributed to shock heating, while in 3 cases it is the line-of-sight component of the CME expansion. For the CME cores we determine the angles between the motion and the plane of the sky, along with the actual heliocentric distances, in order to provide quantitative estimates of projection effects.

Subject headings: Sun: corona — Sun: coronal mass ejections (CMEs) — Sun: UV radiation

1. INTRODUCTION

The continuous monitoring of solar activity by the EUV Imaging Telescope (EIT; Delaboudiniére et al. 1995) and the Large Angle and Spectrometric Coronagraph Experiment (LASCO; Brueckner et al. 1995) aboard the *Solar and Heliospheric Observatory* (*SOHO*) has greatly expanded our understanding of coronal mass ejections (CMEs). The CME morphology is often a three-part structure, with a bright circular front surrounding a dark void in which a bright prominence core is embedded (Webb 1988; Kahler & Hundhausen 1992; Hundhausen 1999). The circular front, also called the leading edge, could be swept-up coronal plasma or plasma carried in the expanding CME magnetic loops or arcades. The void is sometimes identified as the magnetic flux rope corresponding to the magnetic clouds seen in interplanetary space, and the bright core is sometimes identified with gas from the ejected prominence.

CMEs with morphology very different from the standard three-part structure are often observed as well, but this can result from projection effects. White-light images can reveal morphologies, speeds, and widths projected into the plane of the sky, but the three-dimensional structure and actual speeds of CMEs cannot be obtained from such observations. The projection effects can be rather severe and can significantly affect the understanding of CME properties, as the recent work by Burkepile et al. (2004) shows. To overcome this limitation, indirect methods have been proposed by several authors. Schwenn et al. (2001) derive a correlation between the radial speed and the projected expansion speed and estimate the travel time of a CME. Correlation between the lateral expansion speed of the halo CMEs and the speed of the ejecta near Earth has been found by comparing LASCO observations with *Advanced Composition Explorer* (*ACE*) and *Wind* data (Dal Lago et al. 2004). Morphologies of structured CMEs in the C2 field of view (FOV) have been related to the orientation and position of the source region's neutral line on the disk (Cremades & Bothmer 2004). Moran & Davila (2004) and Dere et al. (2005) discuss a promising technique based on the analysis of single-view polarization images to infer the three-dimensional (3D) structure of CMEs. The polarization technique gives an average position along the line of sight for each pixel in the image, but there is an ambiguity between background and foreground positions.

If a geometry of the CME is assumed, the projected heights and speeds can be related to the actual ones. Thus, Sheeley et al. (1999) considered halo CMEs as 3D spherical shells and estimated that the actual speed for a 40° angular width is as large as 3 times the projected values. More recently a cone model has been used to estimate the geometrical and kinematic properties of a 3D halo CME (Zhao et al. 2002; Xie et al. 2004). In this model the CME front is a 3D hemispherical thin shell located at the base of a cone with its apex situated at disk center. The projection of the hemisphere on the plane of the sky (POS) varies from a circular to an ellipsoidal shape depending on the direction of the cone axis and angular width of the CME. One the other hand, extended arcade-like structures have been inferred from white-light (Cremades & Bothmer 2004) and UV (Ciaravella et al. 2003) observations.

It is now widely accepted that the front-side halo CMEs are very well correlated with geomagnetic disturbances (Brueckner et al. 1998; Cane et al. 2000; Gopalswamy et al. 2000; Webb et al. 2000; Zhang et al. 2003). Thus, an important open question in the study of CMEs, and in particular of halo CMEs, is the detection of CME-related shocks in the white-light images. It has been matter of debate which feature of the CME corresponds to the shock. There have been several hypotheses: the shock is located at the leading edge of the CME or is ahead of the apparent CME front (Hundhausen 1987), or as an alternative possibility, Wagner & MacQueen (1983) proposed that in addition to a shock ahead of the front, a blast wave is moving through the ejected material.

Sharp edges have been taken as evidence of shocks at the CME leading edge, but without measurements of the local magnetic field or density or the support of MHD models (Dryer et al. 1979; Vourlidas et al. 2003), it is not possible to prove the presence of a shock from white-light images. Vourlidas et al. (2003) used MHD models to support the identification of shocks, but even

[1] Istituto Nazionale di Astrofisica, Osservatorio Astronomico di Palermo, Piazza del Parlamento 1, 90134 Palermo, Italy.
[2] Harvard-Smithsonian Center for Astrophysics, 60 Garden Street, Cambridge, MA 02138.
[3] Air Force Research Laboratory, VSBXS, 29 Randolph Road, Hanscom AFB, MA 01731.

TABLE 1
SUMMARY OF WHITE-LIGHT AND X-RAY DATA

	LASCO				Flare			
Date	First Appearance[a] (UT)	Speed (km s^{-1})	Width (deg)	Speed (UV) (km s^{-1})	Onset (UT)	Peak (UT)	Location (deg)	Magnitude
1998 Jun 11	10:29 (3.76)	1223	177	1200	09:57	10:27	E limb	M1.4
2000 Mar 29	10:54 (3.15)	949	Halo	643	Back	Back	SE limb	...
2000 Apr 10	00:30 (2.34)	409	Halo	226	23:26	23:42	S14, W01	M3.1
2000 Apr 23	12:54 (4.94)	1187	Halo	1029	Back	Back	NW limb	...
2000 May 11	23:26 (3.25)	716	141	636	22:21	22:24	...	C3.6
2000 Jun 28	19:32 (6.43)	1198	>134	1433	18:48	19:10	N20, W90	C3.7
2000 Aug 12	10:35 (3.85)	662	168	644	09:45	09:56	W limb	M1.1
2000 Sep 12	11:54 (2.83)	1550	Halo	1022	11:31	12:13	S17, W09	M1.0
2000 Oct 22	01:27 (3.73)	1024	236	893	22:30	01:17	S30, E90	EPL
2000 Oct 24	08:50 (3.89)	800	Halo	688	08:04	09:32	E(SE) limb or behind	C2.3
2000 Oct 26	16:50 (3.30)	359	145	478	15:55	16:11	S20, E64	C8.5
2000 Nov 03	18:26 (2.52)	291	Halo	195	18:35	19:02	N02, W02	C3.2
2001 Feb 15	13:54 (3.24)	625	Halo	574	13:08	14:16	N07, E12	B8.8
2001 Mar 24	20:50 (4.33)	906	Halo	589	19:35	19:55	N15, E22	M1.7
2001 Apr 02	22:06 (5.92)	2505	244	2023	21:32	21:51	N17, W78	X20.0
2001 Dec 13	14:54 (3.32)	864	Halo	...	14:20	14:30	N16, E09	X6.2
2002 Apr 21	01:27 (3.32)	2393	Halo	2393	00:43	01:51	S14, W84	X1.5
2002 May 21	21:50 (2.76)	853	135	860	21:20	21:39	N17, E38	M1.5
2002 Jul 09	18:44 (3.5)	1076	Halo	1389	Back	Back	...	...
2002 Jul 15	20:30 (4.54)	1151	Halo	1117	19:59	20:08	N19, W01	X3.0
	21:30 (4.32)	1300	>188	893	21:03	21:32	N19, W01	M1.8
2002 Jul 18	08:06 (4.40)	1099	Halo	1200	07:24	07:44	N19, W30	X1.8

[a] Units for the values in parentheses are $R_{\odot}$.

then the poor constraint on the assumed adiabatic index, γ, leaves some uncertainty.

UV spectra of CMEs can provide significant insight into the 3D structures: the line-of-sight speeds obtained from the Doppler shifts of UV lines, combined with the projected speeds, provide the angles between the motion and the plane of the sky along with the actual heliocentric distances. Spectra can also diagnose the presence of shocks at the CME fronts: line profiles carry information on the bulk expansion and thermal status of the CME material. The number of UV observations of CMEs is not as large as those by white-light coronagraphs because the Ultraviolet Coronagraph Spectrometer (UVCS) can only observe CMEs through its long narrow slit. However, the events observed so far can add significantly to our knowledge of halo CMEs. In this paper we present a catalog of halo and partial halo CMEs detected by UVCS from 1997 October to 2002 July, in terms of their spectroscopic properties. Thus far, UV spectra of CMEs have been analyzed one event at a time because of the great differences among CMEs and among the observing sequences employed. Considering the important results from statistical studies of CMEs with LASCO, this paper is meant to begin the study of UV observations of CMEs as a class. We discuss the typical brightness, Doppler shifts, and line widths of these events and summarize the nature of each event and its observed spectrum in the Appendix.

The paper aims to clarify the nature of the CME front and to determine CME morphology using the different perspective of halo CMEs as compared to limb events. We investigate the question of whether the leading edge corresponds to a shock front, finding evidence that it does in at least seven events. We also investigate the morphology of the leading edge, comparing conical, spherical, and arcade geometries. As part of this study, we derive the angle of the CME axis from the POS and the actual, as opposed to the projected, heliocentric distances for CME core material.

Section 2 describes the white-light, radio, and UV data. An overview of the spectral data diagnostics and Doppler velocity interpretation is discussed in § 3. The results are presented in § 4 where the projection effects, the intensities, the morphology, and the shock diagnostics are discussed. A summary is given in § 5. Finally, in the Appendix we describe the individual CMEs.

2. DATA DESCRIPTION

This paper presents all of the halo and partial halo events in the period 1997 October–2002 July for which the UVCS slit was at the right position at the right time to detect the CME front. However, as we discuss later, in a few cases the front was not detected. We used the list of halos and partial halos as given in the CME catalog[4] to find the corresponding UVCS data, although, as pointed out by Cremades & Bothmer (2004), some of the angular sizes listed in the CME catalog may be overestimated. Because we are interested in CME shocks, we also include brief summaries of the type II radio emission and solar energetic particle (SEP) fluxes. Aside from the 22 events described in this paper, UVCS observed the cores of many other halos and partial halos. Thus, the total number observed in the period 1997 October–2002 July is 53.

Table 1 shows the general characteristics of the events. The first four columns list the date of the observation, time (height), speed, and width of the events as taken from the CME catalog. In the fifth column is the POS speed obtained from LASCO images of the portion of the CME front detected by UVCS. The last four columns give information on the associated flare (or prominence eruption): onset and peak time, the location of the source, and the magnitude of the flare.[5] Of the 22 CMEs presented in this paper, 13

[4] Available at http://cdaw.gsfc.nasa.gov/CME_list.
[5] See http://www.sec.noaa.gov/Data/index.html#indices.

TABLE 2
SUMMARY OF RADIO AND SEP DATA

	Metric Type II Burst					WAVES Type II Frequency			*Wind* 20 MeV	
Date (1)	Station (2)	Start (UT) (3)	Stop (UT) (4)	Intensity (5)	Range (MHz) (6)	Start (UT) (7)	End (UT) (8)	Range (kHz) (9)	Onset (UT) (10)	Peak Intensity (11)
1998 Jun 11	SVTO	1006.0	1018.0	2	35U–85U	1015	10:20	8000–4000	NONE	...
	POTS	1010.9	1018.6	3	40X–70	...	...	...	...	...
2000 Mar 29	NONE	...	...	...	...	...	...	...	NONE	...
2000 Apr 10	CULG	2338.0	2347.0	1, 2	30–120	2315	2345	4500–1000	NONE	...
	HIRA	2338.0	2345.0	2	40–120	...	...	...	...	...
	LEAR	2338.0	2344.0	3	38–80	...	...	...	...	...
	PALE	2338.0	2346.0	2	25–??	...	...	...	...	...
2000 Apr 23	NONE	...	...	...	...	NONE	...	...	1530	0.02
2000 May 11	NONE	...	...	...	...	0100	230	750–450	NONE	...
2000 Jun 28	SGMR	1858.0	1905.0	2	30–80	NONE	...	...	2030	0.002
	HOLL	1903.0	1911.0	1	25–144	...	...	...	...	...
2000 Aug 12	...	...	...	2	...	NONE	...	...	1030	0.03
2000 Sep 12	IZMI	1133.0	1149.8	2	25X–180	1200	1220	14000–60	1330	2
	SGMR	1142.0	1147.0	2	30–60	...	...	...	...	...
	SVTO	1143.0	1213.0	1	25–48	...	...	...	...	...
2000 Oct 22	NONE	...	...	...	...	400	500	14000–6000	NONE	...
2000 Oct 24	NONE	...	...	...	...	...	...	NONE	NONE	...
2000 Oct 26	NONE	...	...	...	...	...	...	...	NONE	...
2000 Nov 03	NONE	...	...	...	...	1835	1845	4000–2500	NONE	...
2001 Feb 15	NONE	...	...	...	...	NONE	...	...	NONE	...
2001 Mar 24	NONE	...	...	...	...	NONE	...	...	NONE	...
2001 Apr 02	SGMR	2149.0	2159.0	2	30–80	2205	230/03	14000–250	2230	15
	HOLL	2151.0	2216.0	2	25–179	...	...	...	...	...
	CULG	2152.0	2157.0	3	28–110	...	...	...	...	...
	HIRA	2152.0	2157.0	3	25–280	...	...	...	...	...
	PALE	2152.0	2238.0	2, 1	25–180	...	...	...	...	...
2001 Dec 13	POTS	1423.5	1443 U	2	40X–170U	NONE	...	...	NONE	...
	BLEN	1428.6	1436.3	3	100X–320	...	...	...	...	...
	HOLL	1429.0	1448.0	1	42–180	...	...	...	...	...
	SVTO	1429.0	1447.0	3	45–180	...	...	...	...	...
2002 Apr 21	PALE	0118.0	0135.0	2	25–180	130	2400	10000–60	0130	20
	CULG	0119.0	0130.0	3	57X–130	...	...	...	...	...
	HIRA	0119.0	0126.0	3	25X–80	...	...	...	...	...
	HOLL	0122.0	0127.0	1	25–180	...	...	...	...	...
	LEAR	0125.0	0136.0	2	25–180	...	...	...	...	...
2002 May 21	HOLL	2128.0	2156.0	1	25–162	...	...	...	NONE	...
	PALE	2128.0	2156.0	1	25–160	...	...	...	...	...
	CULG	2129.0	2145.0	3	57X–160	...	...	...	...	...
	HIRA	2129.0	2157.0	3	25X–140	...	...	...	...	...
2002 Jul 09	POTS	0908.4	0909.7	2	130–170U	...	...	...	...	...
2002 Jul 15	NONE	...	...	...	...	2115	500/16	5000–175	NONE	...
	NONE	...	...	...	...	...	...	...	NONE	...
2002 Jul 18	POTS	0742	0758	3	40X–450	2055	2140	6000–3000	NONE	...
	SVTO	0744.0	0801.0	2	25U–86U	...	...	...	...	...
	IZMI	0744.8	0802.4	2	25X–170	...	...	...	...	...
	LEAR	0747.0	0753.0	2	25U–92U	...	...	...	...	...

are full halos and 9 are partial halos. Four CMEs originated from limb sources, four from behind or very close to the limb, and two were within 16° from the limb. Nine CMEs had sources on the disk. The source of the 2000 May 11 event has not been identified.

Table 2 gives the type II radio bursts reported in Solar-Geophysical Data that are associated with the CMEs. Columns (2), (3), and (4) give the reporting station and onset and end times of the type II bursts. In some cases the times for one station will include two separate bursts reported by that station. Cases of no reported type II bursts may include periods with no observations. Column (5) gives the reported burst intensity, and column (6) gives the observed frequency range, where U indicates uncertainty and X indicates the limit of the observing frequency range. Reports of the *Wind* WAVES type II bursts are taken from the WAVES Web site.[6] The reported WAVES start and stop times are given in columns (7) and (8), and the observed frequency range is given in column (9). Associated peak intensity 20 MeV SEP events are taken from the Goddard Space Flight Center (GSFC) EPACT instrument on *Wind* and are listed in column (10) with onsets given to the nearest hour and peak intensities in column (11) in photons cm^{-2} s^{-1} sr^{-1} MeV^{-1}.

[6] Available at http://lep694.gsfc.nasa.gov/waves/waves.html.

TABLE 3
SUMMARY OF UVCS OBSERVATIONS

	UVCS									
DATE	Height ($R_\odot$)	P.A. (deg)	Exposure Time (s)	Slit Width (arcsec)	Spatial Binning (arcsec)	Detection Time (UT)	Observed Spectral Lines	Detection Wide Profile	Spectral Lines in the Front
1998 Jun 11[a]	1.78	45	100	84	21	10:11	O VI, Lyα, Si XII	Yes	O VI, Si XII
2000 Mar 29	3.64	90	180	28	21	11:16	O VI, Lyα, C III	No	...
2000 Apr 10	2.35	293	120	14	21	02:40	O VI	No	...
2000 Apr 23	1.89	225	120	42	21	12:33	O VI, Lyα, Lyβ	Yes	O VI
2000 May 11	3.11	225	120	42	21	23:33	O VI, Lyα, C III	No	...
2000 Jun 28	2.35	295	120	14	21	19:00	O VI, Lyα, Lyβ, C III, O V	Yes	O VI
2000 Aug 12	2.35	282	120	14	21	10:14	O VI, Lyα	Yes	O VI, Lyα
2000 Sep 12	2.56	135	120	42	21	12:11	O VI, Lyα, Lyβ, Lyγ, C III, O V	Yes	O VI
2000 Oct 22	1.63	100	120	28	21	00:42	O VI, Lyβ, Lyγ, C III	Yes	O VI
2000 Oct 24	3.10	90	120	42	21	08:44	O VI, Lyα, Lyβ	Yes	O VI
2000 Oct 26	1.63	100	120	28	21	15:57	O VI, Lyα, Lyβ, Si XII, Fe XVIII	No	...
2000 Nov 03	1.46	200	200	14	42	19:49	O VI, Lyβ, Lyγ, C III	No	...
2001 Feb 15	2.90	0	600	21	42	13:54	O VI, Lyα	Yes	O VI
2001 Mar 24	2.16	16	300	21	42	20:08	O VI, Lyα	Yes	O VI, Lyα
2001 Apr 02	1.99	223	600	14	42	21:56	O VI, Lyα	Yes	O VI, Lyα
2001 Dec 13	2.46	349	300	21	42	14:23	O VI, Lyα, C III, O V, Si XII	Yes	O VI
2002 Apr 21	1.64	262	120	28	42	01:09	O VI, Lyα, Lyβ, Si XII, Fe XVIII	No	...
2002 May 21	1.95	46	200	42	42	21:38	O VI, Lyβ, Si XII, Al XI	Yes	O VI, Si XII, Al XI
2002 Jul 09	1.71	270	120	21	21	18:24	O VI, Lyα, Lyβ, Lyγ, C III	Yes	O VI, Lyα
2002 Jul 15	3.62	0	120	42	21	20:34	O VI, Lyα, Lyβ, C III	No	...
	2.56	0	120	42	21	21:15	O VI, Lyα, Lyβ, C III	Yes	O VI
2002 Jul 18	2.11	0	120	42	21	08:08	O VI, Lyα, Lyβ, C III	No	...

[a] LYA detector data are available and the slit width is 14″. The Lyα, Lyβ, and Lyγ are the H I Lyman lines. The O VI is the oxygen doublet $\lambda\lambda$1032, 1037. C III, Si XII, O V, Al XI, and Fe XVIII are λ977, λ520 (λ499), λ1218, λ550, and λ974, respectively.

Finally, the UVCS observations are in Table 3. Aside from the date, we list the slit height where the CME was first detected, the polar angle (P.A., measured from north pole) where the slit was centered, the exposure time for each spectrum, the slit width, the spatial binning, and the time when the CME was first detected. The spectral lines in which the CME material was detected are listed in the eighth column. The detection of the front and the spectral lines where the front was detected are in the last two columns. In 14 events the front, or a portion of it, was detected in UV spectra. It is important to mention that many CMEs listed in the table were also observed at other heights.

For each event in Table 1 the LASCO C2 image and the UVCS slit position where the front (if any) was detected are shown in Figures 1–4. In order to show the morphology of the event, we often used C2 images taken at later times than those listed in Table 1.

3. THE ULTRAVIOLET SPECTRA

In this section we describe the main characteristics of UV spectra and related diagnostic tools to study the CMEs.

UVCS is a slit spectrometer that can observe the solar corona from 1.5 up to 10 $R_\odot$ at any polar angle. The 42′ long slit can be up to 84″ wide. The spectrometer was optimized to detect the H I Lyα line and the O VI $\lambda\lambda$1032, 1037 doublet, but many other lines can be also detected in the range 945–1270 Å (473–635 Å in second order; for a detailed description see Kohl et al. 1995). The observation of a CME requires placing the entrance slit at the right time and location in the corona to get spectra of the event as it crosses the FOV of the slit. The spectra are two-dimensional images where the vertical axis is the coordinate along the entrance slit and the horizontal axis is the wavelength dispersion direction. Examples of UVCS spectra are shown in Figure 5. The observations described in this paper include a wide range of UVCS instrument parameters. Spectral resolutions varied from 0.18 to 0.6 Å and exposure times ranged from 120 to 600 s. CMEs observed with long exposure times (300 and 600 s) cannot be used to obtain any reliable conclusion on the nature of the front because other parts of the CME could have been detected along with the front material (see § 4.4). Some events were observed during the daily synoptic scans, which spend short times at several heights. Others were observed during CME watches that maintained one position for hours.

As a CME enters the slit, line intensity changes are detected in the spatial and spectral directions. In general, the spectra emitted by different parts of the CME are different. The evolution of a spectrum during a CME observation is shown in Figure 5. The top panel shows a typical spectrum of the quiet corona in the Si XII λ520 line, O VI $\lambda\lambda$1032, 1037 doublet, and H I Lyβ. In the middle panel the faint and broad emission in O VI and Si XII lines is the CME front. The bright Doppler-shifted knots in the bottom panel are typical CME core structures.

In the UV spectra, we define the more structured material in terms of knots/threads and Doppler shifts as the core. An example is shown in Figure 6. In this figure the two panels show two portions of the spectrum. The two wavelength ranges at the bottom and top of the right panel are for direct and redundant paths. The brightest line in this panel is the H I Lyα from the redundant path. The core material is usually cold, as evidenced by narrow line widths and the presence of ions such as C III λ977 and Si III λ1206 typical of prominence material. However, there are events, like the 2000 October 26 CME in Table 1, in which the core material was detected in the [Fe XVIII] λ974.85 line, which forms at 6×10^6 K.

The UV spectra provide several important diagnostics that have been used for the analysis of the CMEs based on Doppler

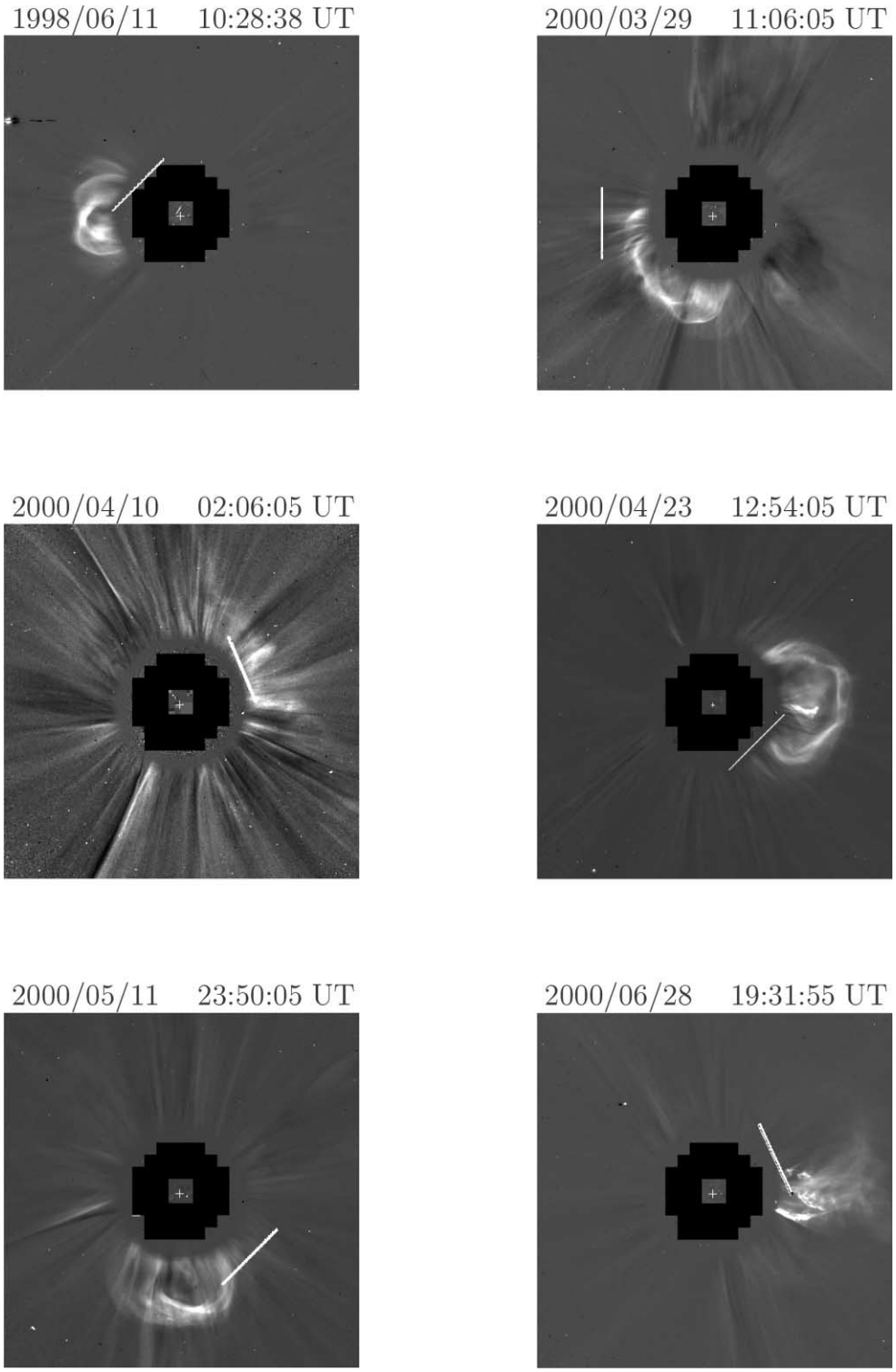

FIG. 1.—LASCO C2 image with the UVCS slit at the position where a CME was first detected, for the 1998 June 11, 2000 March 29, 2000 April 10, 2000 April 23, 2000 May 11, and 2000 June 28 events. The UVCS detection time is generally different than the C2 image shown in the figure (see Table 3).

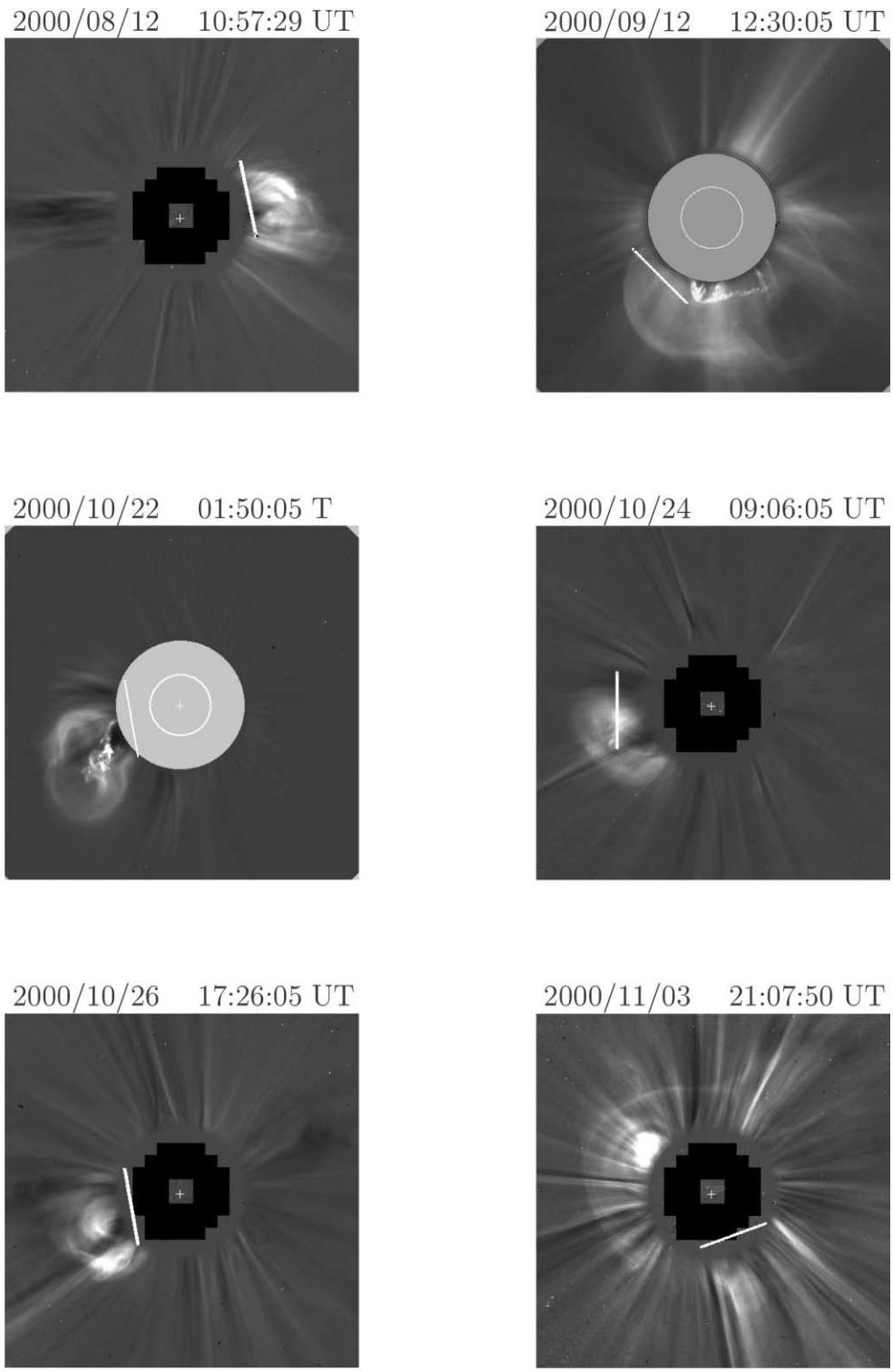

FIG. 2.—Same as Fig. 1, but for the 2000 August 12, 2000 September 12, 2000 October 22, 2000 October 24, 2000 October 26, and 2000 November 3 events.

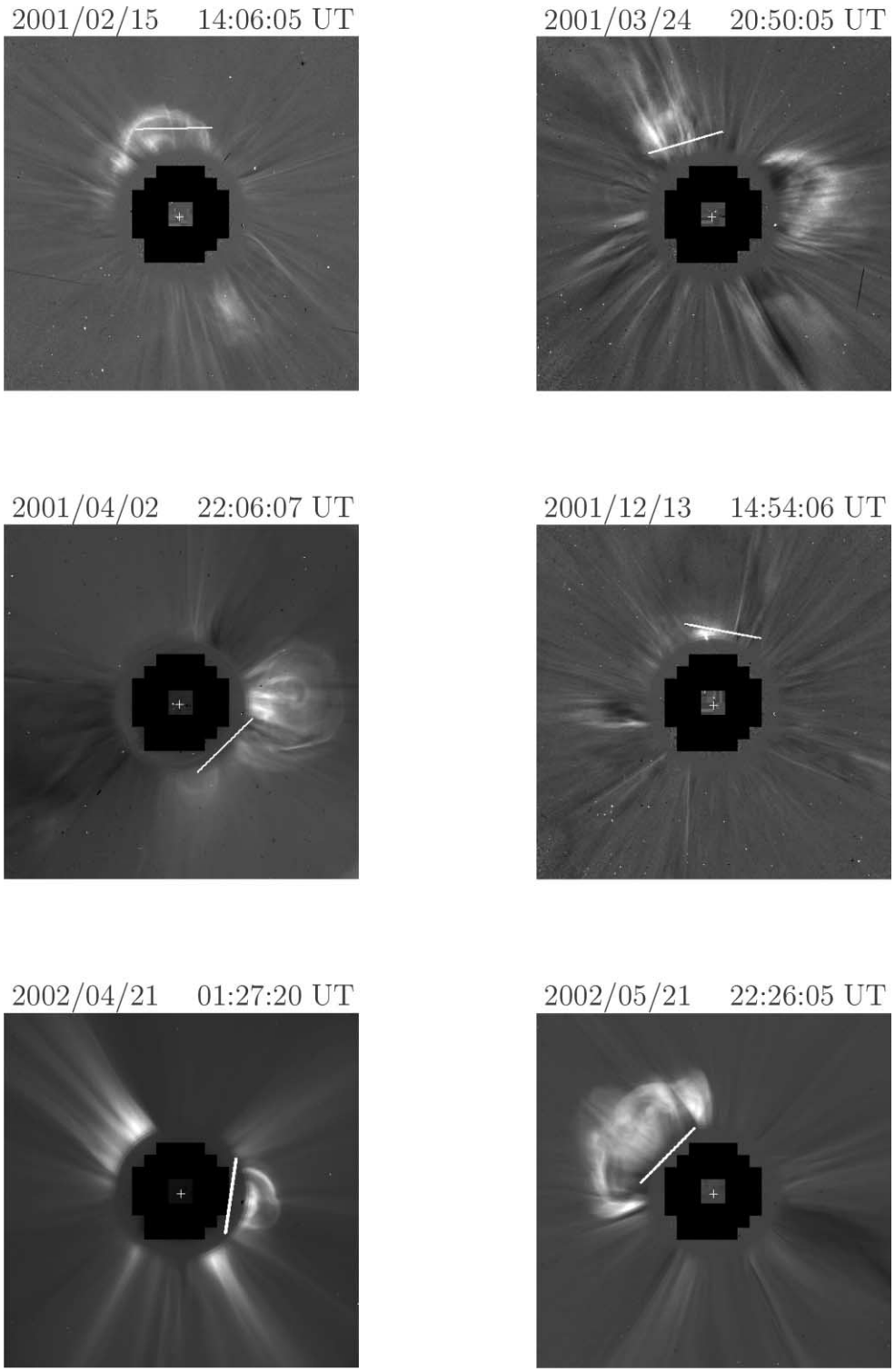

FIG. 3.—Same as Fig. 1, but for the 2001 February 15, 2001 March 24, 2001 April 2, 2001 December 13, 2002 April 21, and 2002 May 21 events.

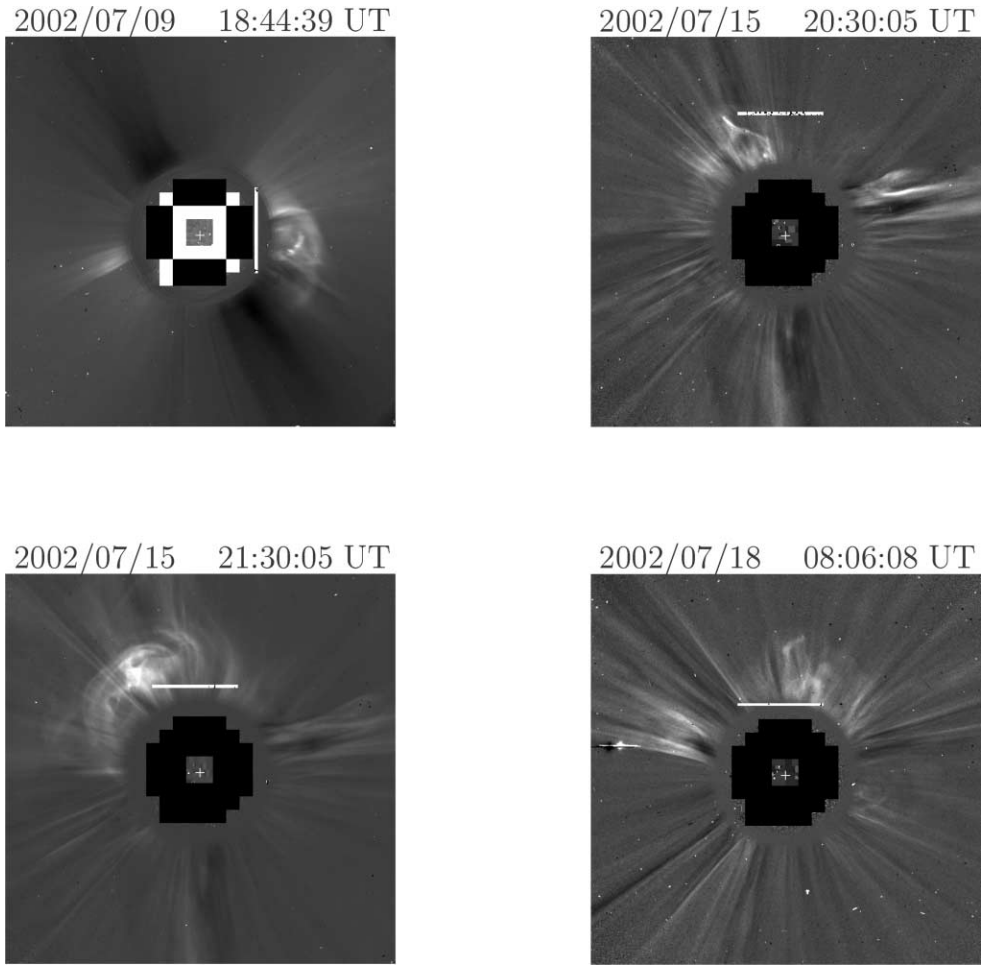

FIG. 4.—Same as Fig. 1, but for the 2002 July 9, 2002 July 15 (20:30:05 and 21:30:05 UT), and 2002 July 18 events.

shifts, line width, and line intensities (Ciaravella et al. 2002; Raymond et al. 2000; Raymond & Ciaravella 2004).

The Doppler shift of the spectral lines provides the component along the line of sight:

$$V_{\rm LOS} = \frac{\Delta\lambda}{\lambda} c, \qquad (1)$$

where c is the speed of light. For spectral lines formed by scattering of radiation from the solar disk, this formula can underestimate the Doppler shift if the material is far from the plane of the sky (Noci & Maccari 1999). Most of the events listed in the tables show large Doppler shifts, such that Doppler dimming greatly reduces any radiative component and the observed emission is collisionally excited.

When $V_{\rm LOS}$ is combined with the LASCO plane-of-sky speed $V_{\rm POS}$, the total speed and the angle with the plane of the sky can be obtained. Knowing the angle, the true height of the observed portion of the CME can be computed (Ciaravella et al. 2005). This is especially important for halo CMEs, as they can be much higher in the corona than they appear in the white-light images. The interpretation of the Doppler velocity is discussed further in the next section.

UV spectra also provide an alternative method to estimate a reliable outflow speed by using the spectral lines with radiative components, such as the O VI $\lambda\lambda$1032, 1037 doublet. The collisional components of the O VI lines have an intensity ratio of 0.5, while the ratio of the radiative components is 0.25 for emitting plasma at rest. The radiative component originates from the resonant scattering of the chromospheric line by the oxygen ions of the corona. As the ions move outward in the corona, the radiative component dims because the solar emission and coronal absorption profiles are Doppler shifted apart. Thus, the line ratio increases and eventually becomes collisional when the outflow speed is such that the absorbing and emitting profiles no longer overlap. However, at higher speeds the nearby lines of C II $\lambda\lambda$1036.34, 1037.02 can pump the radiative component of the λ1037 line at outflow speeds of 170 and 370 km s^{-1}, respectively (Noci et al. 1987; Li et al. 1998). In very fast CMEs pumping of the λ1037 line by λ1032 ($v = 1650$ km s^{-1}) and the λ1032 line by Lyβ ($v = 1810$ km s^{-1}) can occur, as for the 2000 June 28 event (Raymond & Ciaravella 2004). Thus, the Doppler shift combined with LASCO speed and the O VI ratio doublet provide two independent diagnostics for the outflow speed of CMEs.

The O VI doublet also provides diagnostics of density (Mariska 1977; Noci et al. 1987; Raymond & Ciaravella 2004). Since the illuminating flux from the disk is known, the intensity of the radiative component fixes the number of O VI ions in the corona. The intensity of the collisional component, combined with the O VI column density and excitation rate, determines the electron density. This is most easily applied to pre-CME coronal densities (Table 5), but it can sometimes be used for CME ejecta.

The analysis of line profiles can be used to diagnose temperature as well as bulk speed of the emitting plasma. Both expansion of the emitting volume and increasing temperature contribute to broadening the line profiles. The comparison of different spectral

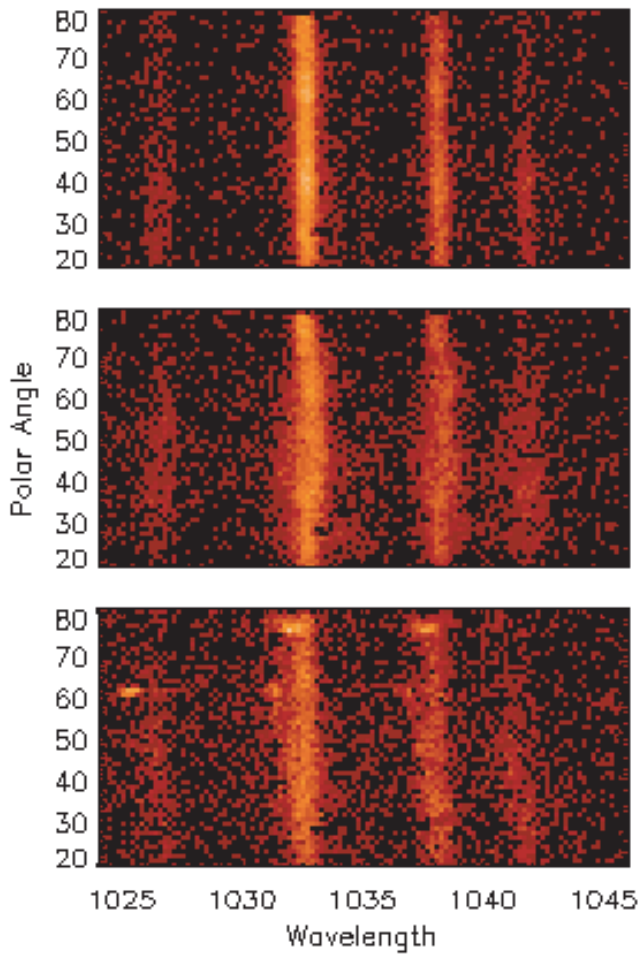

FIG. 5.—Spectra of the 2002 May 21 CME taken at 1.95 $R_\odot$. The vertical axis shows the coordinate along the slit in polar angle measured from the north pole. The horizontal axis is the wavelength dispersion direction. The spectrum includes Si XII λ520, O VI $\lambda\lambda$1032, 1037, and H I Lyβ lines. The top, middle, and bottom panels are spectra of the pre-CME corona, the CME front, and the CME core, respectively. The broadening of the line in the middle panel is due to the passage of the front.

lines and the estimate of the expansion speed are required to disentangle the two effects (Ciaravella et al. 2005; Raymond et al. 2000). It is often possible to obtain interesting upper limits on the proton temperature from the Lyα profile alone.

The heating due to the passage of a shock is detected in terms of broad wings mainly in the nonneutral ions. The neutral atoms, like the hydrogen, should not be directly affected by an MHD collisionless shock. Those atoms can interact by ionizing collisions with the hot electrons of the plasma, a process that can require several tens of minutes, or by resonant charge transfer with fast shocked protons. This process is effective in a timescale of minutes and can contribute significantly to the heating of neutrals. Thus, in the UVCS spectra the presence of a shock front is more likely to be detected in the spectral lines of the brightest ions such as the O VI doublet, but broadening of the H I Lyα line, if present, provides a direct diagnostic of the proton temperature behind the shock. Detections of shocks in UV spectra have already been reported for four CMEs (Raymond et al. 2000; Mancuso et al. 2002; Raouafi et al. 2004; Ciaravella et al. 2005).

3.1. *Doppler Velocity Interpretation*

As discussed in the previous section, the Doppler shift of the spectral line provides the component of the CME speed along the

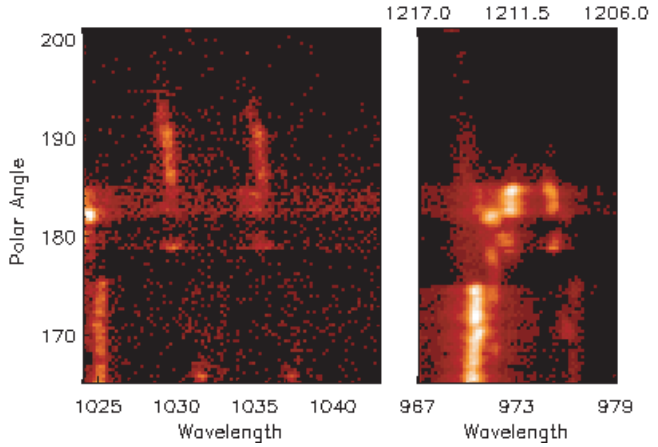

FIG. 6.—Spectrum of the 2000 September 12 CME core taken at 3.62 $R_\odot$. The vertical and horizontal axes are as in Fig. 5. The two panels show two portions of the spectrum. In the right panel the direct and redundant wavelength ranges are shown at the bottom and top of the panel, respectively. In the left panel are the O VI $\lambda\lambda$1032, 1037 doublet and H I Lyβ lines, while in the right panel are the C III λ977 and H I Lyα lines.

LOS. Once we have a value for $V_{\rm LOS}$, we can compare it with $V_{\rm POS}$, but the meaning of this comparison deserves some discussion. The simplest model would be ejection at constant velocity, for example, ballistic motion at a speed substantially above the escape speed. In that case, arctan ($V_{\rm LOS}/V_{\rm POS}$) gives the angle Ψ of the motion to the plane of the sky, and it also gives the true heliocentric distance of the observed plasma: $H = H_{\rm POS}/\cos\,\Psi$. This is a good approximation for CME core material and for expanding magnetically confined loops.

Interpretation of the Doppler shift of the CME front is more subtle. If the front is a spherical shell, as assumed by Sheeley et al. (1999), or a hemispherical shell, as in the cone model by Zhao et al. (2002), the apparent front will be the line of tangency between the shell and the line of sight, as this is the location of largest column density. As far as the Doppler shift of the front material, the two models are very similar. To describe the Doppler shift behavior as a function of the line-of-sight direction, we use a more general cone model in which the apex of the cone can be located anywhere on the solar disk. We refer to this model as the "ice cream cone model." Figure 7 shows as an example of the ice cream cone model with three different line-of-sight directions.

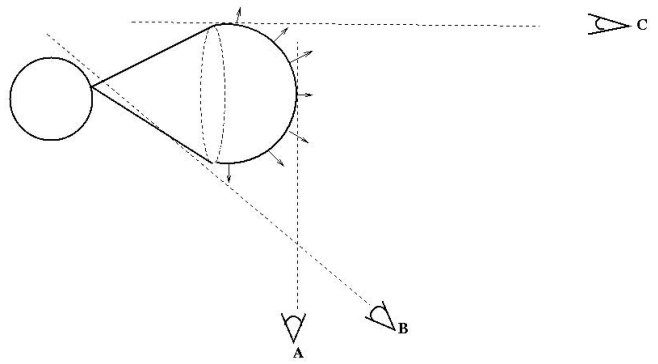

FIG. 7.—CME ice cream cone model and component of the front speed along the line of sight, for a halo event (C) and a limb event (A). The cone model describes the motion of the base of the cone indicated by the dashed ellipse. The line of sight B is nearly tangent to the edge of the cone.

For a cone axis orthogonal to the disk and close to disk center, the line of sight is tangent to the surface close to the intersection of the cone with the hemisphere (LOS C in Fig. 7). If the leading edge consists of coronal material swept up by a shock or a compression wave, the motion of the gas and the CME front itself is perpendicular to the surface of the hemisphere. In the neighborhood of the tangency to the line of sight, the region observed in a halo CME, it is nearly transverse to the radial direction. Thus, this model predicts that the Doppler velocity will generally be much smaller than the speed in the plane of the sky for halo CMEs that originate near disk center. For events that occur close to the limb (LOS A in Fig. 7), the motion is again nearly perpendicular to the line of sight, so again $V_{\rm LOS}$ is much smaller than $V_{\rm POS}$. A large Doppler shift will be seen if the CME is not symmetric, for instance, if only the front or back side is seen. In that case, the angle Ψ given above presents a reasonable approximation for the true position of the emitting plasma, while for events originating at disk center, the plasma can be much farther from the plane of the sky than would be estimated from $H_{\rm POS}/\cos\Psi$. In the latter case the estimate will be a lower limit to the actual heliocentric height. Thus, the Doppler shift of the core material is more useful for estimating Ψ, but the Doppler shift of the front can help test the picture of the CME expansion shown in Figure 7.

The alternative possibility is that the gas is not swept-up coronal material, but plasma carried outward in expanding coronal loops. This could be material of the preexisting arcade-like magnetic structure overlying the filament, or it could be material that has been injected from the current sheet into a "bubble" at the outer edge of the flux rope (Lin et al. 2004). In that case, the plasma motion is perpendicular to the line of sight for a limb event (LOS A), and the Doppler shift will be small. On the other hand, a halo event should show a substantial Doppler shift because the plasma motion is primarily radial rather than perpendicular to the CME surface (LOS C in Fig. 7).

Another case arises if the LOS direction is nearly tangent to the cone edge as B in Figure 7. A Doppler shift corresponding to the outflow speed along the cone should be observed over many exposures in coronal lines. Also, if the event is caught early enough, a Doppler shift corresponding to the lateral expansion of the CME, as is often seen as streamer deflection, may be observed. This material should have an ionization state similar to that of the ambient corona, but the Doppler shift sets it apart from the background coronal emission.

4. RESULTS

In this section we describe the overall characteristics of the 22 CMEs listed in Table 1. Individual events are described in greater detail in the Appendix. For the CMEs where the front was detected (see Table 3 and the Appendix) we use a two-Gaussian fit to separate the background corona emission from the front emission. As shown in Figure 5, the broad profile of the front overlaps the much brighter and narrower profile of the background corona. After correcting for the instrument profile (Kohl et al. 1997), we used a two-Gaussian fit with the narrow component fixed to the width and centroid of the pre-CME line profile, except in a few cases where the centroid had to be shifted by 1 pixel to obtain a good fit or when the spectrum obtained at a different height had to be used. The broad component is that emitted by the front material. Profiles are shown in Figures 8 and 9. In many cases the fits are not unique because of the small number of counts available. We comment on some of these cases later in the paper.

4.1. *Projection Effects*

In this section we summarize the main results of the analysis of UV spectra and discuss the implications for the geometry and kinematics of CMEs. In Table 4 we list some of the measured parameters. The second through fifth columns give the LOS speed of the portion of the front observed by UVCS and the height at which it was measured, the POS speed, the computed angle with the plane of the sky, and the true heliocentric distances. The POS speeds of the portion of the front detected by UVCS are described in § 2. The Doppler shift of the front is computed as the shift between the narrow and broad component of the two-Gaussian fit (see Figs. 8 and 9).

For the CME cores we list the maximum Doppler shift and the height at which it was observed, the POS speed, the minimum and maximum angle with the plane of the sky, and the corresponding minimum and maximum heliocentric distances. Positive and negative values indicate redshifts and blueshifts, respectively. The POS speed of the core is computed by measuring the distance between the CME source and the position of the first core material detected by UVCS and dividing by the difference in time between the activity onset (see Table 1) and the time of UVCS first detection. In four CMEs in which the source was either on the back side or not identified we used the POS speed of the front (third column). The core speeds are generally lower than the front speeds as the core usually remains inside the front. Thus, the angles computed using the front speeds are upper limits ($\Psi_{\rm max}$) to the true values while those computed using the speed derived by comparison of EIT and UVCS observations are lower limits ($\Psi_{\rm min}$) to the true angles. Negative angles are measured toward the observer.

4.1.1. *CME Fronts*

In 14 CMEs we detected the front as broad faint emission superimposed on the narrower coronal emission. In many cases the front was detected for more than one exposure and its Doppler shift and extent along the slit changed from one exposure to another. The Doppler shifts listed in Table 4 are the difference between the centroids of the narrow and broad components of the two-Gaussian fits. A range of values would be more appropriate, but for the purpose of this paper it is important to remark that the Doppler shifts of the fronts are generally much lower than those detected in the CME core. This is intrinsic to the nature of the CME front. The outward expansion speed of a circular front has its maximum component along the LOS in the central part of the front if the front is observed along the lines of sight C of Figure 7. The LOS component decreases away from the CME axis. If the front is observed along the LOS A of Figure 7, the maximum Doppler shift component comes from the flank of the front, where the motion is parallel to the LOS.

Except for five CMEs, the UVCS slit was located away from the axis of the CME. This may explain the low values (see Table 4) of the LOS speeds as this portion of the front moves mostly perpendicular to the line of sight. Therefore, the Doppler shift of a portion of the CME front is not very representative of the LOS speed of the whole front, and the derived heliocentric distances are lower limits to the true values.

During the 2001 February 2, 2001 March 24, and 2002 May 21 events, the slit was centered on the CME front and the derived angles are most probably closer to the actual values. Considering the uncertainties in the measured speed, the angles with the POS of front and prominence core in 2001 February 2 are in good agreement. In the 2002 May 21 event, the CME structure appeared to be formed by several loops with different orientations.

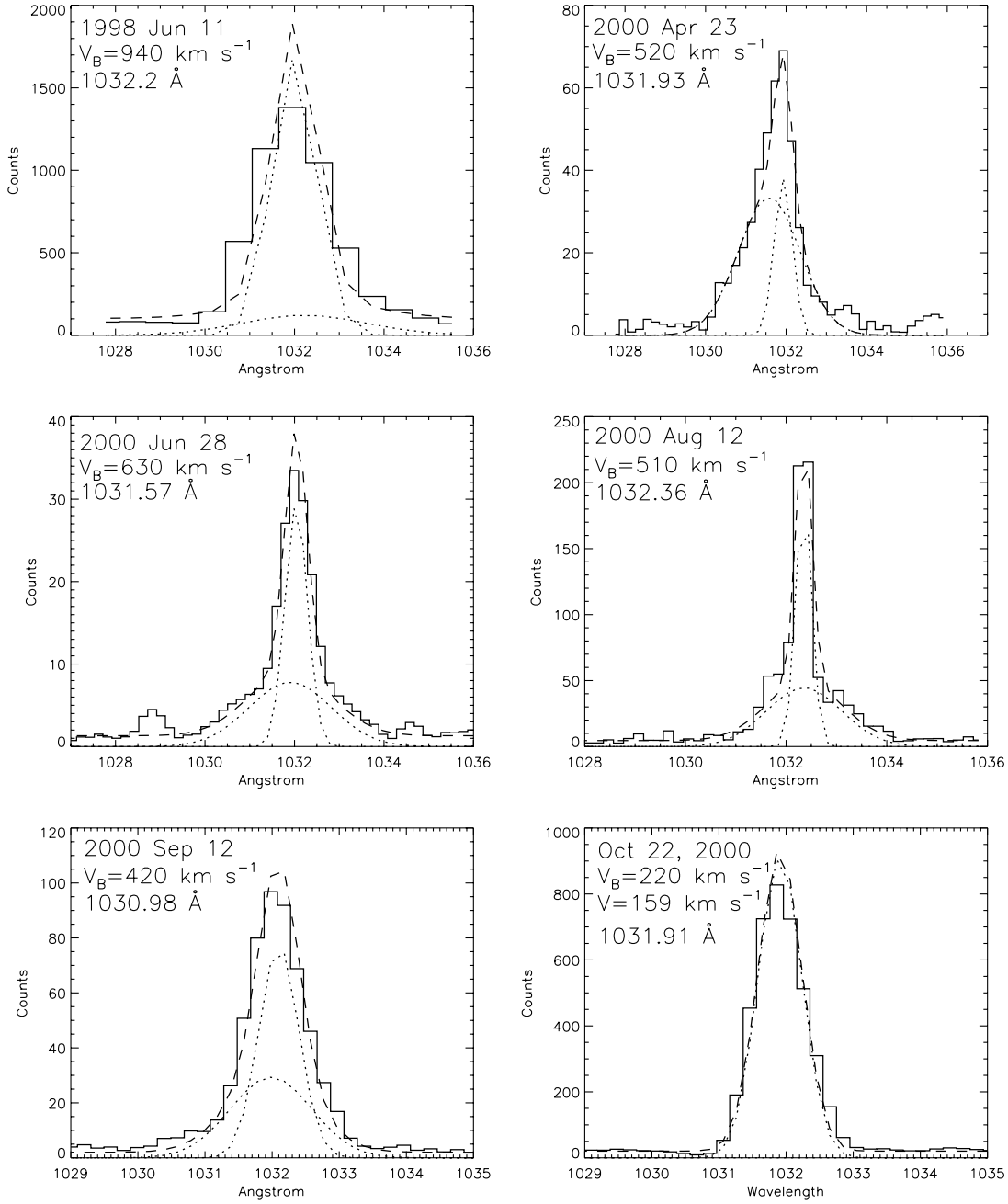

FIG. 8.—O VI λ1032 line profile at the front (*solid line*). The dashed line shows the results of the two-Gaussian fit with a narrow and a broad profile (*dotted line*).

Its 3D structure is far from spherical, and a more detailed analysis of the evolution of the broad component is required to understand its morphology. The 2002 July 9 event was on the back side, but the portion of its front detected by UVCS was traveling toward the Earth at speed greater than 240 km s^{-1}. This can be understood as the opening of surrounding streamers to form the cone (Fig. 7).

Overall, the observations show that the centroid Doppler speeds of halo CME fronts are much smaller than the plane-of-sky speeds (Table 4). This supports the idea that the front is swept-up coronal material rather than plasma carried in expanding magnetic loops, as discussed in § 3.1, and that the schematic shown in Figure 7 is a reasonable description of the front geometry. We use that information to estimate the contribution of bulk expansion to the line widths.

To interpret the measured line widths at the CME fronts, we need to differentiate between bulk expansion and thermal broadening. For a spherical shell expanding from the limb of the Sun (see Fig. 10), the velocity extremes will be $\pm V \sin\theta$, where θ is the angle between the vertical and the line connecting the CME site to the intersection of the line of sight with the bubble. Thus, the full width at zero intensity (FWZI) of the line emitted by the material along the LOS is $2V \sin\theta$. If the thickness of the bubble is small, as in Figure 10 and probably the case for CME fronts, and the spectral resolution high or the expansion speed very large, the two components from the front and back side of the shell will be detected as separate lines. This is most probably the case of the 2002 April 21 event. In all other cases a broadening of the line is seen. The FWHM of the line is less than half the FWZI, both because of the integration over the azimuthal angle around

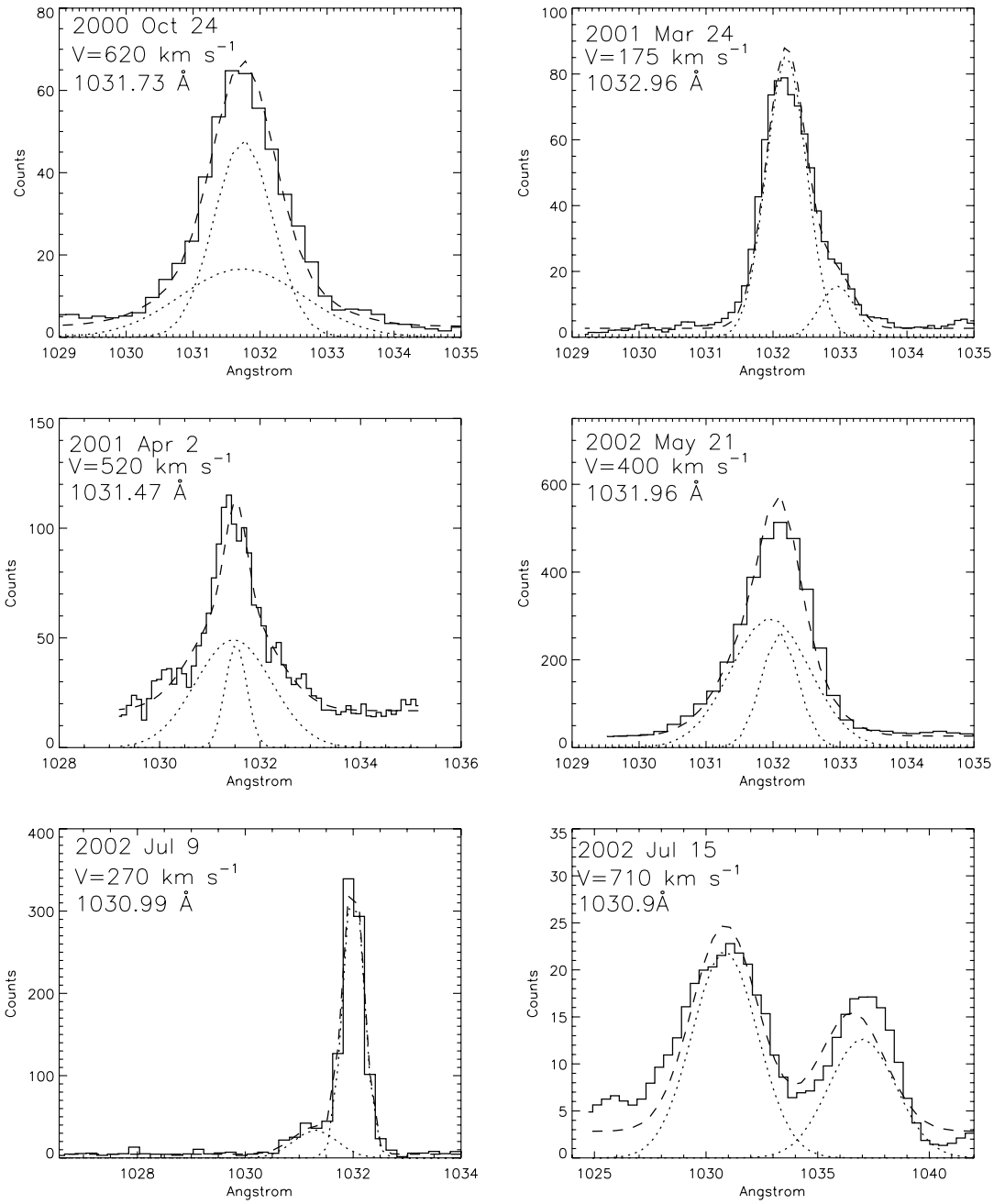

FIG. 9.—Same as in Fig. 8, but for six different CMEs (see label in each panel).

the vertical line and because of the finite thickness of the bubble emission. Figure 10 shows the front at the time Δt_1. At the time Δt_0 the front was tangent to the slit. The slit is marked by the rectangle along the LOS. For an observation that integrates over time $\Delta t = \Delta t_1 - \Delta t_0$, the exposure time of UVCS, from when the bubble first reaches the spectrograph slit, the portion BC of the front is detected and an upper limit to the FWHM is

$$\mathrm{FWHM} < 2V_{\mathrm{CME}} \int_0^{\theta} \int_0^{\pi} \sin\theta \cos\phi \, d\theta \, d\phi$$
$$\sim 2V_{\mathrm{CME}} \frac{\Delta t}{\Delta t_1} \frac{2}{\pi}, \qquad (2)$$

where we used $\langle \int_0^{\pi} \cos\phi \, d\phi \rangle = 2/\pi$. Here Δt_1 is the travel time of the CME from the source (O in Fig. 10) to the height B.

For a slit located 1 $R_{\odot}$ above the solar surface, an integration time of up to 120 s, and a CME speed of 10^3 km s^{-1}, the FWHM due to the bulk expansion speed is less than 200 km s^{-1}. The speed V_{CME} is the true outflow speed of the CME. However, for the purposes of this paper we used the POS speed obtained from LASCO images. Aside from the approximations discussed so far there are other causes that can make the previous estimate an upper limit to the true value: within the exposure time we do not know when the front enters the slit, thus the effective time the front is inside the slit FOV could be less than Δt; the fraction of the front observed can be small. The slit is not centered on the CME, so the integration of the azimuthal angle is smaller; if only the flank of the front is observed, the component of the expansion speed is along the LOS, but as the CME decelerates, the broadening of the line decreases with time.

TABLE 4
LINE-OF-SIGHT AND PLANE-OF-SKY SPEEDS

	FRONT				CORE					
DATE	V_{LOS}[a] (km s^{-1})	V_{POS} (km s^{-1})	Ψ_{min} (deg)	H_{min} ($R_\odot$)	max (V_{LOS})[a] (km s^{-1})	V_{POS} (km s^{-1})	Ψ_{max} (deg)	Ψ_{min} (deg)	H_{max} ($R_\odot$)	H_{min} ($R_\odot$)
1998 Jun 11	+60 (2.00)	1200	>+3	>2.03	+179 (3.24)	198	+42	+8	4.37	3.28
2000 Mar 29	...	643	...	...	+690 (2.91)	643	...	+47	4.27	4.27
2000 Apr 10	...	226	...	...	−230 (2.65)	162	−55	−46	4.60	3.78
2000 Apr 23	+100 (2.10)	1029	>+6	>2.11	+690 (2.08)	1029	...	+34	2.50	2.50
2000 May 11	...	636	...	...	+58 (2.07)	636	...	+5	2.08	2.07
2000 Jun 28	−100 (2.39)	1433	<−4	>2.40	−1200[b] (2.40)	1231	−44	−40	3.35	3.13
2000 Aug 12	0 (2.36)	644	>0	>2.36	...	...	...	...	...	...
2000 Sep 12	−320 (2.57)	1022	<−17	>2.69	−1040[b] (3.84)	237	−77	−45	17.2	5.48
2000 Oct 22	0 (1.80)	893	>0	>1.80	+346 (1.84)	63	+79	+21	10.2	1.97
2000 Oct 24	0 (2.60)	688	>0	>2.60	...	...	...	...	...	...
2000 Oct 26	...	478	...	...	0 (1.63)	272	0	0.	1.63	1.63
2000 Nov 03	...	195	...	...	−29 (1.52)	142	−12	−8	1.55	1.54
2001 Feb 15	−145 (2.95)	574	<−14	>3.04	−230 (3.12)	418	−29	−22	3.56	3.36
2001 Mar 24	−220 (2.61)	589	<−20	>2.79	...	...	...	...	...	...
2001 Apr 02	−16 (2.10)	2023	>0	>2.10	...	...	...	...	...	...
2001 Dec 13	<−58 (2.60)	864	<−4	>2.61	−550 (2.52)	150	−75	−32	9.60	2.99
2002 Apr 21	...	2393	...	...	...	...	...	...	...	...
2002 May 21	−41 (2.03)	860	<−3	>2.03	−520 (2.16)	433	−50	−31	3.37	2.52
2002 Jul 09	−240 (1.83)	1389	<−10	>1.86	+980 (1.72)	1389	...	+35	2.10	2.11
2002 Jul 15	...	1117	...	...	−810 (3.14)	1000	−39	−35	4.04	3.88
	−340 (2.60)	893	<−20	>2.78	−810 (2.82)	1795	−24	−42	3.09	3.81
2002 Jul 18	...	1200	...	...	−920 (2.13)	451	−64	−37	4.84	2.68

[a] The values given in parentheses are in units of $R_\odot$.
[b] Redshift material was also detected.

Comparing the FWHM computed from the above formula with the widths of spectral lines observed in fronts, we conclude that the widths of the O VI lines in the 2000 October 22, 2001 March 24, and 2002 July 9 events are due to the LOS component of the bulk expansion.

4.1.2. *CME Cores*

We can use V_{LOS} and V_{POS} of the Doppler cores to estimate the angle of the ejection from the plane of the sky. To the extent that the core material lies near the center of the CME, this angle also pertains to the CME axis. The angles are shown in Table 4, with the following caveats:

1. The CME core was detected in all but five CMEs. For four of the nondetections the slit was centered on the CME and would have detected the core if it had been present, but during the 2001 April 2 CME the slit was located on the side of the front away from the prominence core (see Fig. 3).

2. The Doppler shifts of the fronts in three events were very small (2000 October 26, 2000 May 11, and 2000 November 3), while the remaining events showed large values. The events on 2000 March 29, 2000 April 23, and 2002 July 9 originated on the back side, and we could not estimate the POS speed from EIT and UVCS data. For these we used the values derived from LASCO; therefore, we have only a lower limit to the angle with the POS. A large opening angle was seen in the 2000 April 10 event. This event originated at disk center and had to travel 2.53 $R_\odot$ in the POS to reach the UVCS slit. If we assume that it was ejected at the time of the flare peak, 23:42 UT, comparison of the POS speed of 162 km s^{-1} with the blueshift of 230 km s^{-1} indicates an angle of 55° from the POS, and the observed plasma was at an actual heliocentric distance of 5.06 $R_\odot$ when observed.

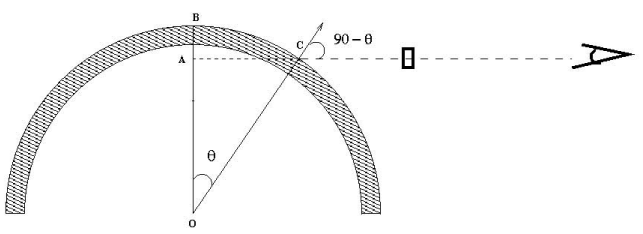

FIG. 10.—CME circular front at height OB above the solar surface. The dashed horizontal line is the LOS direction, and the thick rectangle marks the UVCS slit.

3. Although the source of the 2000 June 28 event was at the limb, the large blueshift detected in the core implies an angle with the plane of the sky of 46° and an actual heliocentric distance of 3.6 $R_\odot$ as compared to the projected distance of 2.32 $R_\odot$. In this event some fragments of the core were redshifted up to 115 km s^{-1}, indicating a broad opening angle.

4. The 2000 September 12 event was also observed at 6 $R_\odot$ and P.A. = 180°, almost centered on the CME. In the first exposure at 14:43 UT, plasma with an average speed in the plane of the sky of 420 km s^{-1} had Doppler shifts into the range −800 to −300 km s^{-1}. Thus, the angle from the plane of the sky ranged from 35° to 62° and the actual heights were 10.5–12.8 $R_\odot$, compared with the projected 6 $R_\odot$.

5. In some cases the projection effects are very severe, such as the 2002 July 18 CME, in which we measured a blueshift up to 920 km s^{-1}, 2 times higher than the average POS speed estimated from EIT and UVCS data. The angle with the POS was as large as 64°, and an actual height was 5 $R_\odot$ as compared to a projected height of 2.13 $R_\odot$. The Doppler shift of the CME core is very small or negligible in the later portion of the event.

6. All limb events with cores had material with large Doppler shifts. The minimum angles with the POS for the CMEs originating

TABLE 5
PRE-CME DENSITIES (10^6 cm^{-3}) AND CME LINE INTENSITIES (10^8 photons s^{-1} cm^{-2} sr^{-1})

		FRONT		CORE	
DATE	PRE-CME DENSITY	O VI[a]	Lyα	O VI[a]	Lyα[a]
1998 Jun 11	3.8–5.5	0.3 (2.0)	...	...	140
2000 Mar 29	0.4–1.0	...	...	10.9 (1.87)	...
2000 Apr 10	1.2–1.6	...	...	2.97	...
2000 Apr 23	...	17.0 (2.10)	...	55.6	169
2000 May 11	...	...	...	249 (1.89)	67300 (1.89)
2000 Jun 28	1.2–1.5	6.76 (2.39)	...	2680	167000
2000 Aug 12	0–2	5.54 (2.36)	...	...	...
2000 Sep 12	...	4.42 (2.57)	...	278 (2.11)	109000 (2.11)
2000 Oct 22	6.9–8.7	<72.3 (1.80)	...	11600	19600
2000 Oct 24	0.86–0.91	0.26 (2.60)	95.8	...	...
2000 Oct 26	6.0–6.4	...	...	...	NA[b]
2000 Nov 03	7.7–9.3	...	...	1910 (1.52)	NA
2001 Feb 15	...	0.06 (2.95)	...	1.36	15.6
2001 Mar 24	3.3–6.5	0.73 (2.61)	...	...	...
2001 Apr 02	0.51–1.4	3.22 (2.10)	170	...	...
2001 Dec 13	0–0.51	0.73 (2.60)	...	252	3470
2002 Apr 21	4.5–5.1	...	...	...	...
2002 May 21	4.7–6.4	7.19 (2.03)	...	8.19	NA
2002 Jul 09	2.6–5.4	50.6 (1.83)	314	290	70000
2002 Jul 15	...	...	...	11.8 (3.62)	62.0 (3.62)
	...	2.17 (2.60)	3.26	5.81	...
2002 Jul 18	4.8–14	...	...	11.7 (2.11)	166 (2.11)

[a] The values given in parentheses are in units of $R_\odot$.
[b] NA: Lyα line was not included in the wavelength range.

at the limb show clearly that in these events the material is also far from the plane of the sky.

4.2. *Intensities*

In the first column of Table 5 are listed the pre-CME coronal densities measured at the same height where the fronts were observed. The densities were derived from the pre-CME O VI intensity ratio as described in § 3. In a few cases the front was observed in the first exposure, and no spectra of the pre-CME corona are available. The remaining columns give the O VI λ1032 and H I Lyα intensities of CME fronts and cores. We indicate with NA the cases in which the line was not included in the detected spectral range. The CME cores were very often detected at several heights. The values listed in the table are measured, whenever possible, at the same slit position where the front was detected. Since front and core are not cospatial along the slit, their absolute heights are different. If many exposures are available at the same height, we select the maximum intensities of the O VI and Lyα lines. The intensities of the CME fronts are the intensities of the broad components of O VI and Lyα lines as obtained from the two-Gaussian fit.

Except for the 2000 October 26 event in which the core was seen in hot lines, all of the remaining cores were seen in cold spectral lines. The lines observed in each CME are listed in the eighth column of Table 3. The presence of cold plasma in the CME core implies that a prominence eruption occurs along with the flare detected at the CME source and that the prominence material is not heated or ionized to coronal conditions. The intensities of Table 5 show that the core material is generally much brighter than the front. The latter is often comparable to or weaker than the background coronal lines. As for the Doppler shift, the brightest material in the core is generally that which is ejected first, and the intensities fade toward the tail of the CME.

The O VI line intensity ratios in some portions of the ejecta of the 2002 July 18, 2002 July 15, and 2002 July 18 events suggest that pumping of the O VI λ1037 line by O VI λ1032 might be present as already detected on 2000 June 28 (Raymond & Ciaravella 2004). In these cases the outflow speed of the CMEs would be as high as 1600 km s^{-1}.

4.3. *Morphologies*

The images in Figures 1–4 show the morphology of the 22 CMEs, and Table 1 gives the associated disk activities that are the most probable sources of the CMEs. The morphologies of the 22 CMEs range from three-part CMEs to diffuse structures without cores to amorphous events. The Doppler shift measurements and the computed angle with the POS provide estimates for the importance of the projection effects.

There are a couple of events in which the behavior of the Doppler shift in the broad line profiles (the front of the CME) suggests that the 3D structure of the CME may be that of a narrow cone in which both the front and back sides of the front are detected. In the 2000 October 22 CME the behavior of the O VI line profiles matches what is expected by a cone structure with the back side of the cone redshifted and the front side blueshifted. The broadening of the O VI profile was first detected on the red side and later on the blue side. In the 2000 October 24 event the two sides of the front were both blueshifted. The back side of the front was caught at 3.1 $R_\odot$, and its broad profile was less blueshifted than the front side of the cone detected at 2.55 $R_\odot$. A more detailed analysis will provide the opening angle of the cone and the angle of the cone axis with the POS.

At the other extreme, the splitting of the O VI profiles in the 2002 April 21 event is exactly what is expected for a more or less hemispherical bubble expanding across the UVCS slit. The splitting starts at the center of the slit and expands toward the ends of

the slit as the bubble moves upward (Fig. 6 of Raymond et al. 2003).

As discussed in § 4.1, the centroid Doppler speeds of the CME fronts are much smaller than the plane-of-sky speeds, supporting the idea that the front is swept-up coronal material. There are several events for which $V_{\rm LOS}$ is a significant fraction of the POS speed, however, and those are good candidates for events in which the front is an expanding loop or arcade. We conclude that for most halo events, the schematic shown in Figure 7 is a better description of the geometry than an expanding arcade picture such as that of Cremades & Bothmer (2004). This may be due to the large actual heights of the material observed in these fronts, since the details of the original ejection become less important as the CME expands, just as a supernova remnant enters a self-similar Sedov phase after it has swept up many times the mass of the original ejection. It may also be that the events observed here are atypically energetic. It is also likely that the bright portion of a CME is arcade material, while we are concentrating on the fainter material at the fronts.

4.4. *Shocks versus Bulk Expansion*

Broadening of the line profiles is a typical signature of the CME front. UVCS detected the CME front in 14 cases. Because of the importance of shock waves in accelerating SEPs and because UV spectra provide unique diagnostics for the physical processes in shocks, it is important to know whether or not the emission arose from shocked plasma.

One indication of a shock is type II radio emission coinciding with the UV detection. The frequency of the type II emission directly determines the density of the preshock and perhaps postshock plasma, and this can be compared with the preshock density at the UVCS FOV determined from the O VI doublet ratio (Table 5), as has been done for the 1998 June 11 event (Raymond et al. 2000). This cannot always be done because the type II emission may be very complex or the frequency information may not be available, as in the 2000 June 28 event (Ciaravella et al. 2005). Moreover, it should be remembered that the UVCS densities are averages along the line of sight.

The second indication of a shock is electron heating. If the shock is relatively efficient in heating the electrons, an increase in the ionization state may be detected, for instance, in an increase in the relative intensity of the Si XII lines. Raymond et al. (2000), Mancuso et al. (2002), and Raouafi et al. (2004) all detected such increases. In principle, however, expanding loops of hot gas might also account for such an increase in the ionization state.

The third indicator is broad line profiles in O VI and other lines. These were the main indications in all four events previously identified as shocks. The thermal widths of lines in the shocked plasma cannot be predicted with great certainty. If the thermal energy is not shared among different particle species, the temperature jump at the shock is proportional to the particle mass, so all species will have the same line width. In a fast shock in the ISM, the ion heating is somewhat below mass-proportional value (Korreck et al. 2004), while in heliospheric shocks it is often equal to or greater than mass-proportional (Berdichevsky et al. 1997; Raymond et al. 1998; K. Korreck et al. 2006, in preparation), but there is considerable scatter from one shock to another. In general, one expects a line width comparable to the shock speed for all species unless the shock is weak.

For each event we estimated the component of the broadening due to the bulk expansion of the front as described in § 4.1. In the 1998 June 11 and 2000 June 28 events the presence of shock was diagnosed by Raymond et al. (2000) and Ciaravella et al. (2005), respectively. In both the 2000 February 15 and 2001 December 13 events, the statistics of the line profiles were too poor to allow any reliable conclusion. The 2001 April 2 event is in principle a good candidate, but the exposure time was too long (600 s) for a CME traveling at 2000 km s^{-1}. Along with the front, a significant fraction of the CME must have crossed the slit because Δt in equation (2) is large.

The front on 2002 May 21 was well centered in the slit and the broad profile was detected in a wide section of the slit. The bulk speed can marginally account for the broadening observed, but the CME is formed by several loops and the resulting front is unlikely to be a circular front. This event needs more detailed analysis to discriminate the geometrical effects from the thermal broadening due to a shock. The possibility that the broadening was due to a shock is supported by the type II radio bursts observed simultaneously (see Table 2) with the UVCS detection of the broad line profile.

Finally, in five events the LOS component of the bulk speed cannot account for the measured width of the lines, and we believe that they are promising candidates for shocks. During the 2000 September 12 event, a type II radio burst in the range 25–48 MHz was observed at the same time UVCS detected the broad profile at the CME front. The substantial Doppler shift of the centroid indicates that this is not simply a shock moving perpendicular to the LOS, however. This observation occurred at the western edge of the event, and it may not be typical of the leading edge shock as a whole.

On 2000 April 23 and 2000 August 12, the broad wings in the O VI lines cannot be attributed to the expansion speed, and they are most probably evidence of shocks. No type II bursts are associated with these events. Only a weak 20 MeV event was detected potentially associated with the 2000 August 12 event. The events of 2000 October 24 and 2002 July 15 (at 21:30 UT) have strong indications of the presence of a shock at the CME front. From our preliminary analysis we conclude that seven events show good evidence for shock heating and two are quite uncertain. The CMEs of 1998 June 11, 2000 October 24, and 2002 May 21 are all east limb source regions and therefore not likely to produce SEP events observed at Earth.

5. SUMMARY AND CONCLUSIONS

So far our knowledge of CMEs is largely based on white-light images. A white-light image is a two-dimensional projection of a 3D structure, so projection effects can have important consequences for understanding such CME properties as geometry, kinetic energy, and mass estimates. In this paper we present a catalog of all of the halo and partial halo CMEs detected by UVCS in the period 1997 October–2002 July for which the slit was at the right time and place for the front or a portion of it to be detected. We used the UV spectra, along with the POS projected heights and speeds, to estimate the angle at which the observed core material moved with respect to the POS and the true heliocentric heights. In 14 cases out of 22 spectra of the front were observed, and we used the Doppler shift to discriminate among different 3D structures. We also measured the intensities and profiles of the UV lines and used them to diagnose the presence of shock at the CME front and the bulk expansion of the observed material.

The main results of our preliminary analysis of the 22 events are as follows:

1. *CME fronts*.—Spectra of the CME front show that its emission is comparable to or weaker than the background coronal emission. Broad line profiles are signatures of CME fronts, but they may or may not be associated with shocks. Seven CMEs

show wide line profiles that cannot be attributed to the LOS component of the bulk expansion speed. For some of them type II bursts are detected as well (see Table 2). These are very promising shock candidates. In three cases the broadening of the lines is due to the bulk expansion.

Doppler shifts detected in the front are generally small, showing that the gas of the fronts is moving mostly transverse to the line of sight. Doppler shifts of the front can be used to discriminate among different 3D flow patterns in the CME front. The LOS component of the expansion speed changes along the front because the velocity is mostly perpendicular to the line of sight at the side of the front, as shown in Figure 7. This may explain the small Doppler shifts detected in the fronts, as the UVCS slit was mostly located away from the axis of the CME. A model of expanding magnetic loops would suggest larger line-of-sight velocities near the CME edges. However, the Doppler shifts of the front are less representative of the true height of the CME than the core material, and we used the Doppler shift of the core to compute the angle of the expansion to the LOS. The Doppler shift evolution of the broad profiles in the 2000 October 22 and 24 events suggests that the 3D structure of the front may be a cone. In many other cases the Doppler shifts and the line widths support an ice cream cone model in which the front expands perpendicular to itself, rather than a model of expanding loops. Doppler shifts of the fronts of events originating at or near the limb are as high as those observed in CMEs originating from the disk.

2. *CME cores*.—Four out of 22 CMEs did show core emission. Except for one event in which the core was seen in hot lines of Si XII and Fe XVIII, all the rest had cores very bright in cold lines. Core material is generally much brighter than the front.

Doppler shifts of the core material are generally much higher than in the front. The related LOS speeds can be comparable to or higher than the POS speeds. The angle with the plane of the sky can be as high as 77°. The events originating at or near the limb do not show a lower LOS speed.

3. *Further analysis*.—Seven promising candidate shock fronts were identified, and further analysis will provide the shock parameters to be compared with those derived from the radio data. This paper also presents several good candidates for understanding the 3D morphologies of CMEs as in Lee et al. (2006) and comparing the UV results with the new technique of 3D reconstruction based on polarization images. The possibility of measuring CME proprieties independently from an assumed geometry is particularly important for space weather predictions that rely on a wide variety of X-ray and optical observations of solar flares and CMEs. The addition of a spectroscopic capability has the appeal that it would be possible to measure line-of-sight velocities directly, rather than inferring them from velocities in the plane of the sky.

We thank Don Reames for providing the EPACT data. This work was supported by NASA grant NAG5-12827 to the Smithsonian Astrophysical Observatory.

APPENDIX

INDIVIDUAL CMEs

1998 June 11.—The EIT, LASCO C1, and UVCS observations of the shock front in this CME were described by Raymond et al. (2000). A large loop system on the northeast limb grew in EIT and LASCO C1 images until it erupted between 09:35 and 09:59 UT. The partial halo event showed an opening angle of about 177° and a speed of 1200 km s^{-1}. UVCS detected the front over about half the slit length at a heliocentric distance of about 2 $R_\odot$. The Si XII emission doubled in brightness, while O VI became brighter by 25% and Lyα dimmed by 10%. These changes, along with type II radio emission and the 900 km s^{-1} line widths of O VI and Si XII, were interpreted in terms of a 1200 km s^{-1} shock of modest Alfvén Mach number, with little thermal equilibration among particle species.

Subsequent exposures at larger heights reveal cool prominence material in Lyα and O VI at a Doppler speed of +180 km s^{-1}. The narrow Lyα profiles of some sections along the slit imply proton kinetic temperatures T_p below 5×10^5 K. The shock front emission was also redshifted by a similar amount. We note that the profile shown in Figure 8 looks different than that in Raymond et al. (2000). For that paper we subtracted off most of the narrow component based on the pre-CME spectra in order to show the broad component more clearly. Here we present a two-Gaussian fit in the same format as that used for the other events.

2000 March 29.—The CME first appeared in LASCO C2 at 11:06 UT and in an 11:15 UT UVCS exposure at 3.64 $R_\odot$ and P.A. = 90°. In the UVCS spectra, the red wings of Lyα and O VI dimmed, while the intensities of the blue wings increased by perhaps 50% at speeds up to −150 km s^{-1} in the southern 9′ of the UVCS slit. These signatures were seen in three exposures between 11:15 and 11:25 UT. UVCS was then moved to P.A. = 135°, where it began its next synoptic scan. At 1.43 $R_\odot$ at 11:31 UT, a bright knot of O VI emission appeared at P.A. = 164.°4 with a Doppler shift of +180 km s^{-1}. In the same exposure a bright knot was seen in Lyα and C III near zero Doppler shift and a P.A. of 155.°2. These are fragments of prominence material. Later the core material was also seen at higher heights at redshifts up to 690 km s^{-1}. The lack of an X-ray flare or a radio burst suggests that this is a back-side event. The drop in emission from the red wings of Lyα and O VI suggests that the CME removed emitting material on the far side of the Sun. The brightening on the blue wing can be interpreted as the transverse opening of the CME, analogous to that seen when streamers are pushed aside by CME expansion.

2000 April 10.—This halo CME came from disk center, and a speed of 410 km s^{-1} was reported for the front. An unusual wide, almost straight front appears in the northwest quadrant of the LASCO C2 image at 02:06 UT. A diffuse feature appears in the lower part of the UVCS slit at 2.35 $R_\odot$ at 02:40 UT and remains until at least 03:01 UT. It is spectrally narrow, probably narrower than the pre-CME O VI emission, and blueshifted by about 230 km s^{-1}. It was rather faint, but it seems to fill the range P.A. = 313°–324° fairly uniformly, although it fades first at lower P.A. The zero-velocity O VI lines are essentially unaffected, and the intensity of the blueshifted λ1032 feature is about the same as that of the average pre-CME. Even when summed over 11 exposures, there are only a few hundred counts in the $\lambda\lambda$1032 and 1037 CME lines, but the doublet ratio in the blueshifted gas is close to the pure collisional value of 2:1. Starting with the beginning of the UVCS exposure sequence at 00:39 UT, the Lyα brightness increases gradually, by about 30% over the course of about an hour. No CME emission is detected in Lyα, presumably because of Doppler dimming, or in C III.

Because the O VI emission was detected so long after the passage of the front (as given by LASCO), and because its line width is small, this is probably CME core material, and UVCS did not detect the front. Its large spatial extent suggests a sheet of gas seen more or less face-on.

2000 April 23.—This west limb halo event showed relatively high speeds of 1190 km s^{-1} according to LASCO and 1030 km s^{-1} from the time of arrival at the UVCS slit. The event originated just behind the west limb, and it appears to involve the active regions about 22° north and south of the equator. A fragment of ejecta is seen by EIT 0.1 $R_\odot$ above the limb at 12:24 UT at the southern edge of the northern active region. The LASCO image shows a wide, somewhat irregular front that suggests a kinked structure. The CME rapidly deflects adjacent streamers to the north and south. UVCS detected the front in O VI emission at the northern end of the slit, which extended from 1.97 $R_\odot$, 242° to 2.29 $R_\odot$, 260°. The previous exposure was obtained at a larger height, so it is impossible to compare CME and pre-CME emission, but a component with $\simeq$520 km s^{-1} FWHM with a 100 km s^{-1} redshift was clearly visible in Figure 8. The CME core was detected at 1.87 $R_\odot$ as a bright knot in the O VI, Lyβ, Lyα, and C III λ977 lines with a redshift of 690 km s^{-1}. The knot was also observed at 1.7 and 1.52 $R_\odot$ but with smaller Doppler shifts.

2000 May 11.—This partial halo event was accompanied by some brightening near disk center in EIT. A C class X-ray flare was seen by the *Geostationary Operational Environmental Satellite* (*GOES*) at about 22:24 UT, but it is hard to determine where it occurred. The CME moved south, reaching the LASCO C2 field at 23:26 UT. At 23:33 UT the UVCS data show no clear broad line profiles when the CME reached the UVCS slit at 3.11 $R_\odot$, although there is some hint of redshifted emission at a very low count rate. This was the first exposure in the sequence at that height, so it is not possible to compare with pre-CME values. In comparison with the subsequent 10 exposures, the two exposures from 23:33 to 23:38 UT showed Lyα brighter on the red wing and fainter on the blue wing by about 30%, but this seems to be just a wavelength shift of about 30 km s^{-1}. Later on, narrow emission profiles of Lyα, C III, and O VI with small Doppler shifts appeared. This is evidently prominence material even though it is not far behind the CME front. Because it is at the western edge of the CME, it might be part of the CME leg.

2000 June 28.—UVCS observations of this event were presented by Ciaravella et al. (2005) and Raymond & Ciaravella (2004). An eruption at the west limb was followed by a partial halo CME that reached 1400 km s^{-1} at a height of 6 $R_\odot$. The front was detected by UVCS at 2.32 $R_\odot$ at 19:00 UT as blueshifted O VI emission with FWHM $= 930 \pm 115$ km s^{-1}. Ciaravella et al. (2005) interpreted this as a shock related to an SEP event an hour later. Cool material that was bright in H I, O V], and O VI lines followed 15 minutes after the front, and it showed redshifts up to 115 km s^{-1} and blueshifts as large as 1200 km s^{-1}. These were used to reconstruct the morphology of the CME in three dimensions (Raymond 2002). Total outflow speeds as high as 1800 km s^{-1} were derived from pumping of the O VI λ1032 by Lyβ and pumping of O VI λ1037 by O VI λ1032 (Raymond & Ciaravella 2004). Analysis of the pumping gave densities in the range of 1.3×10^6–4×10^7 cm^{-3} in different strands of ejected plasma.

2000 August 12.—This partial halo event probably originated in an M class flare near the west limb. Both O VI and Lyα show broad velocity components, with centroids consistent with zero LOS speed. The O VI λ1032 profile shown in Figure 8 is the sum of two exposures covering 10:18–10:22 UT, integrated over the northwestern half of the UVCS slit. It shows a 510 km s^{-1} wide component, which may not be Gaussian. This might suggest that bulk motions account for a significant part of the line width.

2000 September 12.—This event has been studied by Suleiman et al. (2005), who compared the chirality inferred from UVCS and magnetogram data with that expected from the chirality predicted from the Martin & McAllister (1997) indicators. Vršnak et al. (2003) studied the magnetic reconfiguration associated with the two-ribbon flare. The CME source is a long filament in the southern hemisphere that started rising at 11:00 and by 11:48 UT was fully erupted. The front reached the C2 FOV at 11:54 UT and moved at a speed of 1550 km s^{-1}. It reached the UVCS slit at 12:11 UT, when broad profiles in the O VI λ1032 line were detected for a few exposures. By 12:35 UT the cold core material entered the UVCS slit as well. Then the core was observed at many heights from 6 to 1.87 $R_\odot$ at several position angles in the O VI doublet, Lyβ, Lyα, C III, and Lyγ lines.

2000 October 22.—The 2000 October 22 partial halo CME was caused by a prominence eruption on the southeast limb. The CME reached the C2 FOV at 00:50 UT, and its front moved at 1024 km s^{-1}. It appears as a conelike structure with a helical prominence core. UVCS first detected the front at 00:42 UT at 1.64 $R_\odot$ as broad O VI profiles in a wide section of the slit. The O VI profile was first broader on the red side and later on the blue side. In the sixth exposure the profile looked symmetric on the blue and red sides, and its FWHM was about 220 km s^{-1}. The O VI line ratio, $I(1037)/I(1032)$, is 0.37 ± 0.01, requiring an outflow speed lower than 120 km s^{-1}. On the other hand, a POS speed lower than 194 km s^{-1} is obtained when EIT 195 Å images and UVCS data are compared.

2000 October 24.—The 2000 October 24 event originated from a prominence eruption located very close to the east limb. In LASCO C2 images the CME appears as a wavy cone, and the front is far from being circular. The white-light images show diffuse material with no sign of a bright core. The speed in the POS is 800 km s^{-1}. UVCS observed about half of the CME, and the detected ejecta appeared as diffuse material with small contrast with respect to the background corona. The front was first caught at 3.1 $R_\odot$ as broad blueshifted O VI profiles and later at 2.55 $R_\odot$ at larger blueshifts. No sign of the bright cold core material is seen behind the front. O VI is the line that best shows the CME material, but intensity variations of Lyα and Si XII were detected as well.

At 3.1 $R_\odot$ the broadening of the O VI line and the increase of Si XII and O VI intensities by about 20% suggest that a shock might be present. A slight decrease in the Lyα intensity is detected as well. When the other edge of the cone is detected at 2.55 $R_\odot$, the line intensities are decreasing, and the broadening we see may be just bulk expansion speed.

2000 October 26.—The CME source was an active region located at S20°, E64° that produced a C8.5 flare starting from 15:55 UT. The front is very faint in the northern part, while the bright southern portion of the front is most probably enhanced by the compression of the preexisting streamer. The core is very compact and bright. This is a partial halo event with POS speed of 359 km s^{-1}. Most of the CME went through the UVCS slit. However, aside from a brightening of the O VI lines along the slit due to the O VI emission during the impulsive phase of the associated flare (J. C. Raymond et al. 2006, in preparation), UVCS did not detect the CME front. The high-temperature lines of Si XII and [Fe XVIII] are detected in the CME core. While Si XII shows an almost monotonic increase, the [Fe XVIII] reaches a peak and then fades away. Si XII and [Fe XVIII] line profiles are broader than the pre-CME corona, but no significant Doppler shift was detected. The bulk expansion of the core most probably caused the broad line profiles.

2000 November 3.—Although the source was very close to disk center, LASCO C2 images show that the eruption was most probably directed toward the northeast quadrant, where the front and the prominence core were very bright. During the CME the UVCS slit was centered at P.A. = 200° at very low heliocentric heights. The spectra did not show significant changes at the passage of the front. However, bright cold material was seen starting from 19:49 UT. This was most probably related to a second eruption seen in the EIT 195 Å image at 19:48 UT in the southeast quadrant. The front of this CME reinforces the previous one so that it appeared as part of the same event.

2001 February 15.—A circular front moving at 625 km s^{-1} appears in C2 at 15:54 UT, later followed by other looplike structures. It became a full halo by 14:30 UT. The source of the CME is in the northeast quadrant, and in EIT the eruption started at 12:48 UT. The UVCS slit was almost centered on the CME. Unfortunately, the exposure time was 10 minutes, unusually long for CME observations. As the CME front reached the slit, broad O VI profiles were detected for two exposures. The small bright loop behind the front is observed in the O VI lines, while Lyα shows bright diffuse emission inside the front. The core material shows blueshift up to 230 km s^{-1}.

2001 March 24.—The CME erupted in EIT 195 Å at 19:48 UT in the northeast quadrant. The C2 images show material flowing along the streamer followed at 20:50 UT by a looplike structure, and at 21:50 UT the event can be seen as a full halo. UVCS observed broadening of O VI and Lyα lines at 2.13 and 2.58 $R_\odot$. No bright cold material has been observed in the UV spectra.

2001 April 2.—An X20.0 flare is associated with this very fast CME, which was observed in C2 as a partial halo at 22:06 UT traveling at a speed of 2500 km s^{-1}. The flare was located very close to the northwest limb. The CME has a typical three-part structure with a very bright core and a relatively faint front.

The UVCS slit was centered at P.A. = 223° and a height of 1.99 $R_\odot$. From this location just the southern flank of the front was detected. As for 2000 October 26, significant increases of the O VI line intensities were detected during the impulsive phase of the flare due to scattering of flare O VI photons from coronal O VI ions (J. C. Raymond et al. 2006, in preparation). Broad line profiles were observed starting at 21:56 UT. Both O VI and Lyα lines show broad components with FWHM of 520 and 390 km s^{-1}, respectively. No significant signs of the core material were observed.

2001 December 13.—The source of the CME is an active region in the northern hemisphere that erupted at 14:24 UT in EIT 195 Å. This CME is first observed in C2 at 14:54 UT above the north pole, and later, after a gap of 1 hr and 30 minutes, the CME was already at the edge of C2 FOV. UVCS detected in two consecutive exposures an increase of the O VI intensities and broad profiles. The broad components have a very few counts, and we could not fit the line profile.

2002 April 21.—This east limb partial halo event was observed by several *SOHO* instruments, as well as the *Reuven Ramaty High-Energy Solar Spectroscopic Imager* (*RHESSI*) and the *Transition Region and Coronal Explorer* (*TRACE*). The UVCS observations are described by Raymond et al. (2003). Although the front had to pass through the UVCS slit during the observing sequence, no broad component was observed. Instead, the O VI and Si XII lines developed velocity-split components near the center of the slit, and the disturbance spread rapidly over the entire slit length. The velocity splitting of the two components, up to 1300 km s^{-1} in the center of the expanding bubble, can be compared with a plane-of-sky speed of 1200 km s^{-1} at the 1.64 $R_\odot$ height of the UVCS slit (Gallagher et al. 2002). The narrow line widths and the gradual acceleration preclude a shock, so this appears to be material in the streamer legs being blown apart by the CME. Type II emission appeared shortly after the CME crossed the UVCS slit, suggesting that the shock developed at about 2 $R_\odot$. [Fe XVIII] emission was detected from a narrow segment of the slit, most easily interpreted as coming from the current sheet that was seen at lower heights in Fe XXIV with *TRACE* (Gallagher et al. 2002). SUMER spectra showed high speeds and strong [Fe XIX] emission (Innes et al. 2003).

2002 May 21.—The 2002 May 21 CME originated from a region very close to the northeast limb, where a flare was detected at 21:20 UT. The region was fully erupted in EIT 195 Å at 21:48 UT. In LASCO the CME appeared at 21:50 UT and became a partial halo traveling at a speed of 853 km s^{-1}. The CME had a thick wavy front, as if it was formed by three or four major loops with different orientations and, as UV spectra show, different directions of motion. As soon as the CME entered the UVCS slit, the O VI and Si XII lines became broader, first in a small section of the slit and then spreading over a larger area. The line profiles showed first a broadening toward the red wing of the profile. Later the broadening was almost symmetric in the blue and red wings. The broad component of the O VI line has an FWHM of 400 km s^{-1} between 21:42 and 21:49 UT. The front is also detected in the Al XI line. The cold prominence core shows up in the O VI and Lyβ lines as narrow bright knots initially blueshifted by 520 km s^{-1}, and then the shift declines to zero. The cold component is also seen at 3.12 $R_\odot$ with no Doppler shift.

2002 July 9.—The CME appeared in C2 at 18:44 UT as an almost circular front with a bright narrow looplike structure in the core. This back-side event moved at about 1400 km s^{-1} in the plane of the sky. Two UVCS exposures at 1.71 $R_\odot$ detected the front starting at 18:24 UT as broad O VI and Lyα profiles. CME core material was observed at 1.7 $R_\odot$ redshifted by up to 980 km s^{-1}, and at 1.52 $R_\odot$ it was still redshifted up to 404 km s^{-1}. At both heights the Doppler shift decreases with time. Some of the cold prominence core was detected at 2.10 $R_\odot$ as well.

2002 July 15.—On 2002 July 15 two major CMEs originated from the same active region on the northern hemisphere. A halo CME at 20:30 UT was followed by a partial halo at 21:30 UT. Both CMEs traveled at high speed, 1100 and 1300 km s^{-1}, respectively. The two CMEs are described as follows:

1. *20:30 UT*.—When the front crossed the UVCS FOV, the slit was at 3.62 $R_\odot$ where few counts are detected in the spectral lines. Only the brightest core material is seen initially, blueshifted by 980 km s^{-1}. Starting from 20:48 UT the core material was observed at 3.01 $R_\odot$, where a highly structured Doppler shift in O VI, Lyβ, Lyα, and C III lines was observed with blueshift up to 580 km s^{-1}.

2. *21:30 UT*.—At 21:16 UT UVCS caught the partial halo CME at 2.55 $R_\odot$ as broad O VI line profiles corresponding to the northern part of the CME front. A small bright knot is seen in the Lyα and Lyβ lines for many exposures and at several lower heights. The broad O VI doublet profiles are shown in Figure 9. We do not have a pre-CME estimate of the coronal density, and this event was moving in the wake of the previous CME. The profiles show very wide wings. The FWHM of the lines is 710 km s^{-1}.

2002 July 18.—The eruption of the active region is seen in EIT 195 Å at 08:00 UT, and the ejecta appeared in LASCO C2 6 minutes later as a complex set of looplike structures preceded by a very faint circular front. Spectral data do not show changes due to the front but only bright cold material. Thus, although UVCS was at the right location, it did not detect the front.

REFERENCES

Berdichevsky, D., Geiss, J., Gloeckler, G., & Mall, U. 1997, J. Geophys. Res., 102, 2623
Brueckner, G. E., et al. 1995, Sol. Phys., 162, 357
———. 1998, Geophys. Res. Lett., 25, 3019
Burkepile, J. T., Hundhausen, A. J., Stanger, A. L., St. Cyr, O. C., & Seiden, J. A. 2004, J. Geophys. Res., 109(A3), 3103
Cane, H. V., Richardson, I. G., & St. Cyr, O. C. 2000, Geophys. Res. Lett., 27, 3591
Ciaravella, A., Raymond, J. C., Kahler, S., Vourlidas, A., & Li, J. 2005, ApJ, 621, 1121
Ciaravella, A., Raymond, J. C., van Ballegooijen, A., Strachan, L., Vourlidas, A., Li, J., Chen, J., & Panasyuk, A. 2002, ApJ, 575, 1116
———. 2003, ApJ, 597, 1118
Cremades, H., & Bothmer, V. 2004, A&A, 422, 307
Dal Lago, A., et al. 2004, Sol. Phys., 222, 323
Delaboudiniére, J.-P., et al. 1995, Sol. Phys., 162, 291
Dere, K. P., Dennis, W., & Howard, R. 2005, ApJ, 620, L119
Dryer, M., Wu, S. T., Steinolfson, R. S., & Wilson, R. M 1979, ApJ, 227, 1059
Gallagher, P. T., Dennis, B. R., Krucker, S., Schwartz, R. A., & Tolbert, A. K. 2002, Sol. Phys., 210, 341
Gopalswamy, N., Lara, A., Lepping, R. P., Kaiser, M. L., Berdichevsky, D., & St. Cyr, O. C. 2000, Geophys. Res. Lett., 27, 145
Hundhausen, A. J. 1987, in Sixth International Solar Wind Conference, ed. V. J. Pizzo, T. Holzer, & D. G. Sime (Boulder: NCAR), 181
———. 1999, in The Many Faces of the Sun, ed. K. Strong, J. Saba, & B. Hausch (New York: Springer), 143
Innes, D. E., McKenzie, D. E., & Wang, T. 2003, Sol. Phys., 217, 267
Kahler, S. W., & Hundhausen, A. J. 1992, J. Geophys. Res., 97, 1619
Kohl, J. L., et al. 1995, Sol. Phys., 162, 313
———. 1997, Sol. Phys., 175, 613
Korreck, K. E., Raymond, J. C., Zurbuchen, T. H., & Ghavamian, P. 2004, ApJ, 615, 280
Lee, J.-Y., Raymond, J. C., Ko, Y.-K., & Kim, K.-S. 2006, ApJ, 651
Li, X., Habbal, S. R., Kohl, J., & Noci, G. 1998, ApJ, 501, L133
Lin, J., Raymond, J. C., & van Ballegooijen, A. A. 2004, ApJ, 602, 422
Mancuso, S., Raymond, J. C., Kohl, J., Ko, Y.-K., Uzzo, M., & Wu, R. 2002, A&A, 383, 267
Mariska, J. T. 1977, Ph.D. thesis, Harvard Univ.
Martin, S. F., & McAllister, A. H. 1997, in Coronal Mass Ejections, ed. N. Crooker et al. (Geophys. Monogr. 99; Washington: AGU), 127
Moran, T. G., & Davila, J. M. 2004, Science, 305, 66
Noci, G., Kohl, J. L., & Withbroe, G. L. 1987, ApJ, 315, 706
Noci, G., & Maccari, L. 1999, A&A, 341, 275
Raouafi, N.-E., Mancuso, S., Solanki, S. K., Inhester, B., Mierla, M., Stenborg, G., Delaboudinière, J. P., & Benna, C. 2004, A&A, 424, 1039
Raymond, J. C. 2002, in From Solar Min to Max: Half a Solar Cycle with *SOHO*, ed. A. Wilson (ESA SP-508; Noordwijk: ESA), 421
Raymond, J. C., & Ciaravella, A. 2004, ApJ, 606, L159
Raymond, J. C., Ciaravella, A., Dobrzycka, D., Strachan, L., Ko, Y.-K., Uzzo, M., & Raouafi, N. E. 2003, ApJ, 597, 1106
Raymond, J. C., et al. 1998, ApJ, 508, 410
———. 2000, Geophys. Res. Lett., 27, 1439
Schwenn, R., Dal Lago, A., Gonzalez, W. D., Huttunen, E., St. Cyr, C. O., & Plunkett, S. P. 2001, Eos Trans. AGU, 82(47), Fall Meet. Suppl., Abstract SH12A-0739
Sheeley, N. R., Walters, J. H., Wang, Y.-M., & Howard, R. A 1999, J. Geophys. Res., 104(A11), 24739
Suleiman, R. M., Crooker, N. U., Raymond, J. C., & van Ballegooijen, A. 2005, in IAU Symp. 226, Coronal and Stellar Mass Ejections, ed. K. Dere, J. Wang, & Y. Yan (Cambridge: Cambridge Univ. Press), 71
Vourlidas, A., Wu, S. T., Wang, A. H., Subramanian, P., & Howard, R. A. 2003, ApJ, 598, 1392
Vršnak, B., Warmuth, A., Maričić, D., Otruba, W., & Ruždak, V. 2003, Sol. Phys., 217, 187
Wagner, W. J., & MacQueen, R. M. 1983, A&A, 120, 136
Webb, D. F. 1988, J. Geophys. Res., 93, 1749
Webb, D. F., Cliver, E. W., Crooker, N. U., St. Cyr, O. C., & Thompson, B. J. 2000, J. Geophys. Res., 105, 7491
Xie, H., Ofman, L., & Lawrence, G. 2004, J. Geophys. Res., 109(A8), 103
Zhang, J., Dere, K. P., Howard, R. A., & Bothmer, V. 2003, ApJ, 582, 520
Zhao, X. P., Plunkett, S. P., & Liu, W. 2002, J. Geophys. Res., 107(A8), 1223